Electronic Research Archive

https://www.aimspress.com/journal/era

ERA, 33(10): 6343–6374.
DOI: 10.3934/era.2025280
Received: 14 August 2025
Revised: 11 October 2025
Accepted: 16 October 2025
Published: 27 October 2025

Research article

Landau-damped dust-acoustic solitary waves in nonthermal plasmas

Abdulaziz H. Alharbi[1,*], M. S. J. Alzahrani[2], W. M. Moslem[3,4] and I. S. Elkamash[4,5]

[1] Department of Mathematics, Jamoum University College, Umm Al-Qura University, Makkah 25375, Saudi Arabia

[2] Mechanical and Industrial Engineering Department, College of Engineering and computing Al-Leith, Umm Al-Qura University, Makkah, Al Lith 28434, Saudi Arabia

[3] Department of Physics, Faculty of Science, Port Said University, Port Said 42521, Egypt

[4] Centre for Theoretical Physics, The British University in Egypt, El-Shorouk City, Cairo 11837, Egypt

[5] Physics Department, Faculty of Science, Mansoura University, 35516 Mansoura, Egypt

* **Correspondence:** Email: ahhrbe@uqu.edu.sa.

Abstract: We utilize a fluid kinetic hybrid approach to analyze dust acoustic wave propagation in collisionless, unmagnetized dusty plasmas, specifically investigating how linear Landau damping effects in the ion population affect weakly nonlinear and weakly dispersive wave behavior. An electron-depleted plasma is considered, consisting of a cold fluid of negatively charged dust particles and two types of ions at different temperatures, modelled by a kappa-type distribution. Anticipating nonlinear solitary waves, a reductive perturbation technique is employed, leading to a nonlinear partial differential equation for the electrostatic potential in the form of a modified Korteweg–de Vries (mKdV) equation, featuring an additional term to account for linear Landau damping of the ions. The solitary wave's amplitude is found to decay with time. A parametric analysis is carried out of the impact of the plasma configuration on the Landau damping rate under the influence of this latter (Landau damping-related) term. The results of this work are highlighted in space plasma, such as that around Enceladus and Saturn's E ring, where the occurrence of Landau damping in combination with a nonthermal ion distribution may affect wave propagation significantly.

Keywords: partial differential equations; numerical solution; solitary waves; nonthermal plasmas; Landau-damped

1. Introduction

Power-law distributions of particle velocities are ubiquitous in various plasma environments, for example, in space plasma [1–3], and in astrophysical plasma [4, 5]. Such distribution functions show the suprathermal departures from the Maxwellian equilibrium. They are often observed in low-density plasmas across the universe, provided that collisions between charged particles are sufficiently rare. They should also be present in the polytropic behavior of plasmas, which includes superstatistics (that is, the superposition of different Maxwell distributions with different temperatures) and diffusive shock acceleration or stochastic acceleration processes [6, 7].

Vasyliunas's [8] groundbreaking research showed that the kappa (κ) distribution function can be used to accurately describe suprathermal particle populations. This (κ)-distribution matches the velocity distribution data that were measured in experiments. Kappa distributions have stronger high-energy tails that follow power-law decay with particle velocity, unlike Maxwellian distributions [9]. Many researchers have looked into how kappa distributions affect different plasma situations. For example, fluid-based methods have been used to study how κ-distributed background populations change excitations at ionic scales [10]. Elkamash and Kourakis [11] studied how multicomponent plasma expands into a vacuum and how ions speed up when superthermal electrons are present, which are described by κ-distributions.

Lazar et al. [12] investigated the long-standing debate on whether the temperature in kappa-distributed plasmas depends on the power-index κ. By contrasting global kappa and dual Maxwellian kappa models using in situ measurements of solar wind electrons, their analysis provides strong evidence for a κ-dependent temperature. The dual Maxwellian kappa model not only offers a better fit to observations but also indicates that suprathermal electrons enhance temperature anisotropy-driven instabilities, leading to systematically lower κ values. Slathia et al. [13] studied the head-on collision of dust ions acoustic multi-solitons in a magnetized plasma consisting of inertial ions, stationary charged dust grains, and superthermal electrons. By applying the extended Poincaré–Lighthill–Kuo (PLK) method and Hirota's bilinear approach, they derived and solved two Korteweg–de Vries (KdV) equations. Their results highlight the significant roles of electron superthermality, density ratios, and magnetic field strength in shaping soliton dynamics and collision-induced phase shifts, with implications for space environments such as Saturn's magnetosphere. Abishek and Michael [14] explored ions acoustic shock waves in Saturn's magnetospheric plasma, composed of superthermal electrons, H^+, O_2^+, and N^+ ions—relevant to plasma originating from Enceladus. Using the reductive perturbation method, they derived the Korteweg–de Vries–Burger equation and solved it via the tanh method. Their analysis showed that electron superthermality, ion densities, temperature, and ion viscosity strongly influence shock waves characteristics. Notably, higher N^+ and H^+ densities enhance the shock's amplitude, while higher κ indices tend to suppress it. A transition from shock to soliton structures was also demonstrated. Jahangir et al. [15] investigated the propagation of nonlinear electron acoustic waves in a four-component magnetized plasma composed of inertial cold electrons, warm drifting beam electrons, trapped superthermal hot electrons, and stationary ions. Employing a reductive perturbation approach, they derived a trapped Zakharov–Kuznetsov equation to examine solitary wave structures. Their results demonstrate how superthermality, electron trapping, and beam parameters influence the solitary profiles, consistent with Viking spacecraft observations in the auroral region. The study provides valuable insight into energy transport and wave dynamics in magnetospheric

environments such as the magnetopause.

Dusty plasmas are systems that have particles that are micron-sized or smaller and get positive or negative charges through different processes, such as thermionic emission, field emission, radioactive processes, impact ionization, and the collection of electrons and ions from the environment [16]. You can find these plasma environments in many different places in space, such as interplanetary regions, interstellar media, molecular clouds, circumstellar environments, cometary atmospheres, planetary ring structures, noctilucent cloud formations, and even on Earth, where charged particles are always present [17–19]. Dusty plasmas can be used in a wide range of fields, such as microelectronics, optoelectronic systems, photonic devices, microelectromechanical structures, material fabrication, and many other industrial and technological applications, such as making small circuit parts and many other things [20–22]. When charged dust grains are added to electron ion plasma systems, they behave very differently than they do without them. Theoretical research has found that low-frequency dust acoustic modes (DAWs) and high-frequency dust ion acoustic oscillations (DIAWs) are possible [23, 24]. After that, scientists looked at both linear and nonlinear dusty plasma dynamics in a variety of plasma settings. Rosenberg and Merlino [25] looked at how charged dust grains affect the stability of ion acoustic waves in dusty negative ion systems, both in the lab and in space. Researchers have looked at how ion dust collisions and ions kinematic viscosity affect the formation of solitary and shock waves in dusty plasmas with negative ions [26]. Elkamash et al. [27,28] looked into electrostatic shock structures in multispecies plasma systems. They included the effects of kinematic viscosity, drag collision processes, and external magnetic fields all at once. Mishra [29] looked into the possibility of low-frequency dust wave phenomena happening near sunlit lunar regoliths that contains two-component dusty plasma systems, specifically positively charged particles inside photoelectron sheaths. The study showed that changes in the charge of dust can change the normal dispersion characteristics of DAW and create ultralow frequency modes that move at slower phase velocities.

Wave particle interactions play crucial roles in many processes seen in plasma systems in labs, space, and astrophysics, as well as many other places, such as the excitation and damping of collective modes, plasma absorption of laser radiation in inertial fusion experiments, the formation of magnetopause boundary layers, the radiation emission of hard X-raysand gamma rays, and the acceleration of charged particles in relativistic regimes [30–33]. One of the most dominant damping mechanisms for waves in the wave particle interaction is Landau damping. Landau [34] showed that the plasma waves in unmagnetized collisionless plasmas suffer damping due to wave particle interaction without any collision between charged particles. Thus, Landau damping does not happen because of random collisions; it happens because energy moves from wave fields to resonant particle oscillations. Ott and Sudan [35] developed a new technique to involve linear Landau damping in studying the nonlinear ion acoustic wave and to investigate how the initial perturbations evolve to form a shock wave. The authors came up with a new governing equation called the modified Korteweg–de Vries equation (mKdV). This equation includes Landau damping effects that happen because of finite electron inertia and dispersive effects that happen because of finite Debye length. Their study showed that Landau damping makes the amplitudes of solitary waves decrease over time. Bandyopadhyay and Das [36, 37] created different evolution equations to study weakly nonlinear and weakly dispersive ion-acoustic waves in magnetized nonthermal plasma with adiabatic warm ions. These equations account for Landau damping effects that happen because of the finite electron-to-ion inertia ratio. They used the multiple time scale method to obtain the solitary wave solutions of these equations

that propagate obliquely to the external magnetic field. Saitou and Nakamura [38] used a multidipole double plasma device to experimentally and numerically investigate the effect of Landau damping on the ion acoustic soliton-like waves. They used radio frequency signal to control the ion heating and hence to control the Landau damping effect in the experiment. The influence of the Landau damping, due to the finite electron ion mass ratio, on a weakly nonlinear and weakly dispersive ion acoustic wave in an electron positron ion plasma, has been examined [39]. Barman and Misra [40] studied the nonlinear theory of DAWs, including the Landau damping effect in an unmagnetized dusty negative ion plasma. They modelled the negative dusty species with fluid equations, and positive and negative ions kinetic Vlasov equations, where at equilibrium the ions obey the Maxwellian distributions. Researchers have looked at how Landau damping of electrons and ions , as well as weak quantum regime effects, affect the propagation of nonlinear ion acoustic waves (IAWs) in unmagnetized collisionless plasma systems [41]. Sikdar and Khan [42] looked at how Landau damping affects nonlinear dust acoustic solitary waves in unmagnetized plasma environments with electrons, ions, and negatively charged dust particles. They did this by looking at how the charge on the dust grains changes. Ghai et al. [43] looked at both analytical and numerical studies of dust acoustic (DA) solitary and shock structures. They included Landau damping effects in dusty plasma systems with two-temperature ions that followed the non-Maxwellian Cairns distribution. They found that nonthermal ion density and temperature have a significant effect on the solitary wave amplitude decaying. Researchers have looked into how electron Landau damping affects the movement of ion-acoustic waves in collisionless, unmagnetized plasma systems with warm adiabatic ions and two types of electrons at different temperatures [44]. Misra et al. [45] looked at how multi-plasmon resonance affects linear and nonlinear electron acoustic waves (EAWs) in quantum plasma environments that are only partially degenerate and have two-temperature electrons that follow Fermi Dirac equilibrium distributions and stationary ion populations. Their results showed that two-plasmon resonance processes are the main way that Landau damping of EAWs happens in quantum plasma systems. Ion acoustic solitary waves (IASWs) in collisionless, unmagnetized plasma were studied by Mushtaq et al. [46] using Landau-type kinetic damping and suprathermal electrons with a kappa distribution. They derived a modified KdV equation with a nonlocal damping component using multiscale perturbation. They found analytical solutions showing a decrease in amplitude. Their study shows how Landau damping and electron superthermality affect IASWs behavior.

This work investigates the effects of non-Maxwellian ion statistics on dust acoustic solitary wave propagation under Landau damping from first principles. We want to understand how wave particle interactions create and move low-frequency electrostatic solitary waves in space plasma, such as those around Enceladus and Saturn's E ring, which indicate dusty plasma. One of Cassini's most astounding findings was that Saturn's moon Enceladus discharges water vapor and ice grains from its south pole, generating a continuous plume that enriches Saturn's E ring and inner magnetosphere. This environment is ionized by plasma interactions with ejected neutral material, supplementing it with charged particles. The plume and E ring both include a high population of dust grains from micrometer to nanoscale sizes. Dusty plasma forms when these grains capture ambient electrons and become negatively charged. Therefore, many electrons get attached to the dust, depleting the free electron population naturally. Due to charge redistribution, plasma's quasi-neutrality is maintained by free ions, negatively charged dust, and fewer free electrons [47, 48]. Space studies have indicated that electron densities in these locations are sometimes substantially lower than ion densities. This imbalance slows

corotating ions and increases thermal ion-charged dust grain coupling in plasma. Thus, the Enceladus plume's interaction with Saturn's magnetospheric plasma creates a unique electrodynamic environment that causes negatively charged dust and electron depletion.

The paper is organized as follows. In Section 2, we present the basic physical model and the underlying assumptions. The nonlinear theory of dust acoustic waves, the derivation of the modified KdV equation, and an approximate soliton solution of the mKdV equation are presented in Section 3. The results and discussion nedded to understand Landau damping and the power-law distribution function on the nonlinear characteristics of DAWs are shown in Section 4. Finally, the findings of the present work are summarized in Section 5.

2. The mathematical model

We investigate a collisionless, unmagnetized dusty plasma that contains no electrons and consists of a negatively charged dust fluid along with two ion species. Both ion populations follow power-law velocity distributions described by κ distributions. Each ion component is characterized by its own temperature (T_1 and T_2) and spectral index (κ_1 and κ_2). The colder ion population is considered to have a significantly greater mass than the hotter one. To simplify the analysis, a one-dimensional (1D) planar geometry is employed, and the cold dust component is modeled using fluid dynamic equations. Dimensional variables carry a tilde.

$$\frac{\partial \tilde{n}_d}{\partial \tilde{t}} + \frac{\partial}{\partial \tilde{x}}(\tilde{n}_d \tilde{u}_d) = 0, \tag{2.1}$$

$$m_d \tilde{n}_d \left(\frac{\partial \tilde{u}_d}{\partial \tilde{t}} + \tilde{u}_d \frac{\partial \tilde{u}_d}{\partial \tilde{x}} \right) = -q_d \tilde{n}_d \frac{\partial \tilde{\phi}}{\partial \tilde{x}}, \tag{2.2}$$

$$\frac{\partial^2 \tilde{\phi}}{\partial \tilde{x}^2} = -\frac{1}{\epsilon_0}(q_1 \tilde{n}_1 + q_2 \tilde{n}_2 + q_d \tilde{n}_d), \tag{2.3}$$

where $q_d = -z_d e$, $q_1 = z_1 e$, and $q_2 = z_2 e$.

Each ion species ($j = 1, 2$) is governed by the collisionless Vlasov equation for the distribution function $\tilde{f}_j(\tilde{x}, \tilde{v}, \tilde{t})$:

$$\frac{\partial \tilde{f}_j}{\partial \tilde{t}} + \tilde{v} \frac{\partial \tilde{f}_j}{\partial \tilde{x}} - \frac{q_j}{m_j} \frac{\partial \tilde{\phi}}{\partial \tilde{x}} \frac{\partial \tilde{f}_j}{\partial \tilde{v}} = 0. \tag{2.4}$$

The number density of species j then follows from

$$\tilde{n}_j = \int_{-\infty}^{\infty} \tilde{f}_j \, d\tilde{v}. \tag{2.5}$$

In (2.1)–(2.5), $\tilde{n}_d$ and $\tilde{u}_d$ are the dust dust's numerical density and velocity, $\tilde{\phi}$ denotes the electrostatic potential ,and $\tilde{x}$ and $\tilde{t}$ are the spatial and temporal coordinates. At equilibrium, quasi-neutrality imposes

$$z_1 n_{10} + z_2 n_{20} = z_d n_{d0}. \tag{2.6}$$

Here, $n_{j0} = \int_{-\infty}^{\infty} \tilde{f}_j^{(0)} \, d\tilde{v}$ is the equilibrium density of species j, with $\tilde{f}_j^{(0)}$ being its equilibrium

distribution. Both ion populations are assumed to be non thermal with the 1D κ equilibrium

$$\tilde{f}_j^{(0)}(\tilde{v}) = \frac{n_{j0}}{v_{\mathrm{th}j}} \frac{1}{\sqrt{2\pi}\,(\kappa_j - \frac{3}{2})^{1/2}} \frac{\Gamma(\kappa_j)}{\Gamma(\kappa_j - \frac{1}{2})} \left(1 + \frac{1}{\kappa_j - \frac{3}{2}} \frac{\tilde{v}^2}{2v_{\mathrm{th}j}^2}\right)^{-\kappa_j}, \tag{2.7}$$

where the (corrected) ion thermal speed is

$$v_{\mathrm{th}j} = \sqrt{\frac{K_B T_j}{m_j}}, \tag{2.8}$$

and $\kappa_j > 3/2$ is the spectral index controlling suprathermal tails. As $\kappa_j \to \infty$, (2.7) reduces to the Maxwell–Boltzmann equilibrium.

We focus on long-wavelength, low-frequency, electrostatic disturbances propagating predominantly along one coordinate. This is the standard setting in reductive perturbation studies of ion dust acoustic type modes, where transverse variations are weak and do not alter the leading balance among nonlinearity, dispersion, and kinetic resonances. The 1D planar reduction provides a controlled asymptotic backbone while remaining widely used in space and laboratory dusty plasma contexts.

To non dimensionalize, we employ the dust scales

$$\lambda_d = \left(\frac{\epsilon_0 K_B T_1}{z_d e^2 n_{d0}}\right)^{1/2}, \quad \omega_{pd} = \left(\frac{z_d^2 e^2 n_{d0}}{\epsilon_0 m_d}\right)^{1/2}, \quad c_s = \omega_{pd}\lambda_d = \left(\frac{z_d K_B T_1}{m_d}\right)^{1/2}, \tag{2.9}$$

and an arbitrary macroscopic length L (defining $\ell = \lambda_d^2/L^2$). The *dimensional* $\to$ *dimensionless* map is

$$\tilde{x} = \lambda_d x, \quad \tilde{t} = \frac{t}{\omega_{pd}}, \quad \tilde{u}_d = c_s u_d, \quad \tilde{\phi} = \frac{K_B T_1}{e}\phi, \quad \tilde{v} = v_{\mathrm{th}1} v, \quad \tilde{n}_d = n_{d0} n_d, \quad \tilde{f}_j = \frac{n_{j0}}{v_{\mathrm{th}j}} f_j. \tag{2.10}$$

Worked normalization of each equation (for more details, see Appendix A). Dust continuity. From (2.1), substitute the map and divide by $(n_{d0}c_s/\lambda_d)$

$$\frac{\partial(n_{d0}n_d)}{\partial(t/\omega_{pd})} + \frac{\partial}{\partial(\lambda_d x)}[(n_{d0}n_d)(c_s u_d)] = 0 \;\Rightarrow\; \frac{\partial n_d}{\partial t} + \frac{\partial(n_d u_d)}{\partial x} = 0. \tag{2.11}$$

Dust momentum. From (2.2), divide by $(m_d c_s^2 n_{d0}/\lambda_d)$

$$\frac{\partial u_d}{\partial t} + u_d \frac{\partial u_d}{\partial x} = \frac{q_d}{m_d}\frac{\lambda_d}{c_s^2}\frac{\partial \tilde{\phi}}{\partial \tilde{x}} = \frac{q_d}{m_d}\frac{\lambda_d}{c_s^2}\frac{K_B T_1}{e}\frac{1}{\lambda_d}\frac{\partial \phi}{\partial x} = \frac{\partial \phi}{\partial x}, \tag{2.12}$$

since $c_s^2 = z_d K_B T_1/m_d$ and $q_d = -z_d e$.

Ion Vlasov. From (2.4),

$$\underbrace{\frac{1}{\omega_{pd}}}_{\sim\epsilon^{3/2}}\frac{\partial f_j}{\partial t} + \underbrace{\frac{v_{\mathrm{th}1}}{\lambda_d}}_{\sim\epsilon^0} v\frac{\partial f_j}{\partial x} - \frac{q_j}{m_j}\underbrace{\frac{K_B T_1}{e\lambda_d}}_{\sim\epsilon^0}\frac{\partial \phi}{\partial x}\underbrace{\frac{1}{v_{\mathrm{th}j}}}_{\sim\epsilon^0}\frac{\partial f_j}{\partial v} = 0. \tag{2.13}$$

Multiplying by $\lambda_d/v_{\mathrm{th}1}$ with the parameter definitions below yields

$$\mu_d = \sqrt{\frac{z_d m_1}{z_1 m_d}}, \qquad Q_j = \frac{z_j}{z_1}, \qquad \mu_j = \frac{m_j}{m_1}, \qquad \theta_j = \frac{T_j}{T_1}, \tag{2.14}$$

and the compact form

$$\mu_d \frac{\partial f_j}{\partial t} + v\frac{\partial f_j}{\partial x} - \frac{Q_j}{\mu_j}\frac{\partial \phi}{\partial x}\frac{\partial f_j}{\partial v} = 0. \tag{2.15}$$

Ion density. Using $\tilde{n}_j = \int \tilde{f}_j \, d\tilde{v}$ with the scalings gives

$$n_j = \frac{1}{n_{j0}} \int \tilde{f}_j \, d\tilde{v} = \frac{1}{n_{j0}} \int \frac{n_{j0}}{v_{\mathrm{th}j}} f_j \, (v_{\mathrm{th}1} \, dv) = \sqrt{\frac{\mu_j}{\theta_j}} \int_{-\infty}^{\infty} f_j \, dv, \tag{2.16}$$

where $\sqrt{\mu_j/\theta_j} = v_{\mathrm{th}1}/v_{\mathrm{th}j}$ arises solely from the velocity scaling.

Poisson. From (2.3), using $\tilde{x} = \lambda_d x$ and $\tilde{\phi} = (K_B T_1/e)\phi$, we have

$$\frac{K_B T_1}{e}\frac{1}{\lambda_d^2}\frac{\partial^2 \phi}{\partial x^2} = -\frac{1}{\epsilon_0}(q_1 n_{10} n_1 + q_2 n_{20} n_2 + q_d n_{d0} n_d), \tag{2.17}$$

and dividing by $(K_B T_1/e)/\lambda_d^2$ with $\delta_j = z_j n_{j0}/(z_d n_{d0})$ and $\ell = \lambda_d^2/L^2$ (with L being the slow scale used later) gives

$$\ell \frac{\partial^2 \phi}{\partial x^2} = n_d - \sum_{j=1}^{2} \delta_j n_j, \qquad \delta_1 + \delta_2 = 1. \tag{2.18}$$

κ equilibrium (normalized)

$$f_j^{(0)}(v) = \frac{1}{\sqrt{2\pi}\,(\kappa_j - \frac{3}{2})^{1/2}} \frac{\Gamma(\kappa_j)}{\Gamma(\kappa_j - \frac{1}{2})} \left(1 + \frac{1}{\kappa_j - \frac{3}{2}}\frac{\mu_j}{\theta_j}\frac{v^2}{2}\right)^{-\kappa_j}, \tag{2.19}$$

whose $\kappa_j \to \infty$ limit is

$$\lim_{\kappa_j \to \infty} \left(1 + \frac{\alpha v^2}{\kappa_j}\right)^{-\kappa_j} = e^{-\alpha v^2}, \qquad \alpha = \frac{1}{2}\frac{\mu_j}{\theta_j}, \tag{2.20}$$

so

$$f_j^{(0)} \to \frac{1}{\sqrt{2\pi}} \exp\left(-\frac{\mu_j}{\theta_j}\frac{v^2}{2}\right) = f_{\mathrm{MB}}. \tag{2.21}$$

Table 1. Mapping between dimensional and normalized symbols, with meanings and scales.

Dimensional	Normalized	Meaning	Scale / definition
$\tilde{x}$	x	Space coordinate	$\tilde{x} = \lambda_d x$
$\tilde{t}$	t	Time	$\tilde{t} = t/\omega_{pd}$
$\tilde{u}_d$	u_d	Dust's fluid velocity	$\tilde{u}_d = c_s\, u_d$
$\tilde{n}_d$	n_d	Dust's density	$\tilde{n}_d = n_{d0}\, n_d$
$\tilde{\phi}$	ϕ	Electrostatic potential	$\tilde{\phi} = (K_B T_1/e)\, \phi$
$\tilde{v}$	v	Particle velocity	$\tilde{v} = v_{\mathrm{th}1}\, v$
$\tilde{f}_j$	f_j	Ion distribution function	$\tilde{f}_j = (n_{j0}/v_{\mathrm{th}j})\, f_j$
$\tilde{n}_j$	n_j	Ion's density (species j)	$\tilde{n}_j = n_{j0}\, n_j$
λ_d	ℓ	Debye length / dispersion	$\ell = \lambda_d^2/L^2$
ω_{pd}	—	Dust's plasma frequency	$\sqrt{z_d^2 e^2 n_{d0}/(\epsilon_0 m_d)}$
c_s	—	Dust's acoustic speed	$\omega_{pd}\lambda_d = \sqrt{z_d K_B T_1/m_d}$
$v_{\mathrm{th}j}$	—	Ion thermal speed	$\sqrt{K_B T_j/m_j}$
—	μ_d	Ion/dust inertia parameter	$\sqrt{z_d m_1/(z_1 m_d)}$
—	Q_j	Charge ratio	z_j/z_1
—	μ_j	Mass ratio	m_j/m_1
—	θ_j	Temperature ratio	T_j/T_1
—	δ_j	Density/charge ratio	$z_j n_{j0}/(z_d n_{d0})$

To examine how nonlinearity, dispersion, and Landau-type damping interact in shaping weakly nonlinear structures (e.g., solitary waves), we introduce a small parameter $\epsilon \ll 1$ and postulate the standard reductive-perturbation ordering

$$\mu_d = \chi_1 \epsilon, \tag{2.22}$$

$$\frac{n_d}{n_{d0}} - 1 = \chi_2 \epsilon, \tag{2.23}$$

$$\ell = \chi_3 \epsilon, \tag{2.24}$$

with $O(1)$ constants $\chi_{1,2,3}$. This scaling balances the following:

- *Quadratic nonlinearity* from the dust fluid (*via* convective terms) at $O(\chi_2^2 \epsilon^2)$.
- *Third-order dispersion* from Poisson (through ℓ) also at $O(\chi_3 \epsilon)$ acting on $O(\chi_2 \epsilon)$ fields.
- *Weak kinetic (Landau) contribution* controlled by $\mu_d = \chi_1 \epsilon$, which enters kinetic closure and generates a Hilbert transform term in the amplitude equation.

3. Nonlinear analysis

We apply the hybrid fluid–kinetic model developed in Section II to explore nonlinear wave propagation in the plasma. To facilitate analytical progress, we employ the reductive perturbation technique [35, 40], introducing the stretched (slow) variables

$$\xi = \epsilon^{1/2}(x - \lambda t), \qquad \tau = \epsilon^{3/2} t, \tag{3.1}$$

where ϵ is a small bookkeeping parameter that measures the weakness of nonlinearity and dispersion, while λ denotes the (a priori unknown) phase speed of the wave.

To keep the wave's amplitude independent from the dispersion and kinetic damping strengths, the smallness of the fluid and potential perturbations is taken to be the same as that of the density perturbation. Accordingly, the dependent variables (the dust's density and velocity, electrostatic potential, and ion quantities) are expanded as

$$\begin{aligned} n_d &= 1 + \chi_2 \epsilon\, n_d^{(1)} + \chi_2^2 \epsilon^2\, n_d^{(2)} + \cdots, \\ u_d &= \chi_2 \epsilon\, u_d^{(1)} + \chi_2^2 \epsilon^2\, u_d^{(2)} + \cdots, \\ f_j &= f_j^{(0)} + \chi_2 \epsilon\, f_j^{(1)} + \chi_2^2 \epsilon^2\, f_j^{(2)} + \cdots, \\ n_j &= 1 + \chi_2 \epsilon\, n_j^{(1)} + \chi_2^2 \epsilon^2\, n_j^{(2)} + \cdots, \\ \phi &= \chi_2 \epsilon\, \phi^{(1)} + \chi_2^2 \epsilon^2\, \phi^{(2)} + \cdots. \end{aligned} \tag{3.2}$$

With stretching (3.1), this choice ensures that the leading-order fluid closure appears at $O(\epsilon^{3/2})$ and that quadratic nonlinearity balances dispersion at the same asymptotic order (the KdV balance). The parameters χ_1 and χ_3 continue to control, independently, the strengths of kinetic damping and dispersion.

Substituting (3.1)–(3.2) into the normalized governing equations (2.11)–(2.18) and collecting the terms of equal powers of ϵ yield the first-order (linear) system

$$-\lambda \frac{\partial n_d^{(1)}}{\partial \tau} + \frac{\partial u_d^{(1)}}{\partial \xi} = 0, \tag{3.3}$$

$$-\lambda \frac{\partial u_d^{(1)}}{\partial \tau} - \frac{\partial \phi^{(1)}}{\partial \xi} = 0, \tag{3.4}$$

$$v \frac{\partial f_j^{(1)}}{\partial \xi} - \frac{Q_j}{\mu_j} \frac{\partial \phi^{(1)}}{\partial \xi} \frac{\partial f_j^{(0)}}{\partial v} = 0, \tag{3.5}$$

$$n_j^{(1)} - \sqrt{\frac{\mu_j}{\theta_j}} \int_{-\infty}^{\infty} f_j^{(1)}\, dv = 0, \tag{3.6}$$

$$n_d^{(1)} - \sum_j \delta_j n_j^{(1)} = 0. \tag{3.7}$$

From (3.3)–(3.4) , we obtain the first-order fluid closure

$$n_d^{(1)} = -\frac{1}{\lambda^2} \phi^{(1)}, \qquad u_d^{(1)} = -\frac{1}{\lambda} \phi^{(1)}. \tag{3.8}$$

Regularization of the resonant kinetic response. Direct integration of (3.5) gives

$$\frac{\partial f_j^{(1)}}{\partial \xi} = \frac{Q_j}{\mu_j} \frac{\partial \phi^{(1)}}{\partial \xi} \frac{\partial f_j^{(0)}}{\partial v} + \varrho(\xi, \tau)\, \delta(v), \tag{3.9}$$

with $\delta(v)$ being the Dirac delta and $\varrho(\xi, \tau)$ being an arbitrary function that reflects the resonance and the lack of uniqueness unless an initial value formulation is adopted. Following standard practice [35, 40],

we retain the formally higher-order time derivative that appears at $O(\epsilon^{7/2})$ under (3.1)–(3.2) as follows:

$$\chi_1\epsilon^2\frac{\partial f_{j\epsilon}^{(1)}}{\partial\tau}+v\frac{\partial f_{j\epsilon}^{(1)}}{\partial\xi}-\frac{Q_j}{\mu_j}\frac{\partial\phi^{(1)}}{\partial\xi}\frac{\partial f_j^{(0)}}{\partial v}=0,\qquad f_j^{(1)}=\lim_{\epsilon\to0}f_{j\epsilon}^{(1)}. \tag{3.10}$$

Fourier transformation of (3.10) in (ξ,τ) leads to

$$\hat{f}_{j\epsilon}^{(1)}=\frac{Q_j}{\mu_j}\frac{k\,\partial_v f_j^{(0)}}{kv-\chi_1\epsilon^2\omega}\,\hat{\phi}^{(1)}. \tag{3.11}$$

Introducing the Landau prescription $\omega\to\omega+i\gamma$ ($\gamma>0$) leads to

$$\hat{f}_{j\epsilon}^{(1)}=\frac{Q_j}{\mu_j}\frac{k\,\partial_v f_j^{(0)}}{(kv-\chi_1\epsilon^2\omega)-i\gamma\chi_1\epsilon^2}\,\hat{\phi}^{(1)}. \tag{3.12}$$

Using the Plemelj formula in the limit $\epsilon\to0$ gives

$$\hat{f}_j^{(1)}=2\,\frac{Q_j}{\mu_j}\,\partial_v^2 f_j^{(0)}\,\hat{\phi}^{(1)}, \tag{3.13}$$

so the inverse transform yields

$$f_j^{(1)}(\xi,v,\tau)=2\,\frac{Q_j}{\mu_j}\,\partial_v^2 f_j^{(0)}(v)\,\phi^{(1)}(\xi,\tau). \tag{3.14}$$

From (3.6),

$$n_j^{(1)}=-C_j^{(1)}\phi^{(1)},\qquad C_j^{(1)}=\frac{\kappa_j-\frac{1}{2}}{(\kappa_j-\frac{3}{2})^{3/2}}\frac{1}{\theta_j}. \tag{3.15}$$

Substituting (3.8) and (3.15) into (3.7) yields the phase speed

$$\lambda=\pm\frac{1}{\sqrt{\sum_{j=1}^{2}\delta_j C_j^{(1)}}}=\pm\frac{1}{\sqrt{\delta_1 C_1^{(1)}+\delta_2 C_2^{(1)}}}, \tag{3.16}$$

where the sign distinguishes right/left propagation. The linear dispersion relation is derived in Appendix A.

The second order and compatibility. Collecting next-order terms leads to

$$-\lambda\frac{\partial n_d^{(2)}}{\partial\xi}+\frac{\partial u_d^{(2)}}{\partial\xi}=-\left(\frac{\partial n_d^{(1)}}{\partial\tau}+\frac{\partial}{\partial\xi}[n_d^{(1)}u_d^{(1)}]\right), \tag{3.17}$$

$$-\lambda\frac{\partial u_d^{(2)}}{\partial\xi}-\frac{\partial\phi^{(2)}}{\partial\xi}=-\left(\frac{\partial u_d^{(1)}}{\partial\tau}+u_d^{(1)}\frac{\partial u_d^{(1)}}{\partial\xi}\right), \tag{3.18}$$

$$v\frac{\partial f_j^{(2)}}{\partial\xi}-\frac{Q_j}{\mu_j}\frac{\partial\phi^{(2)}}{\partial\xi}\frac{\partial f_j^{(0)}}{\partial v}=\chi_1\lambda\frac{\partial f_j^{(1)}}{\partial\xi}+\frac{Q_j}{\mu_j}\frac{\partial\phi^{(1)}}{\partial\xi}\frac{\partial f_j^{(1)}}{\partial v}, \tag{3.19}$$

$$n_j^{(2)} - \sqrt{\frac{\mu_j}{\theta_j}} \int_{-\infty}^{\infty} f_j^{(2)}\, dv = 0, \tag{3.20}$$

$$\chi_3 \frac{\partial^2 \phi^{(1)}}{\partial \xi^2} - n_d^{(2)} + \sum_j \delta_j n_j^{(2)} = 0. \tag{3.21}$$

From (3.17), (3.18) and (3.8),

$$\frac{\partial n_d^{(2)}}{\partial \xi} = -\frac{2}{\lambda^3}\frac{\partial \phi^{(1)}}{\partial \tau} + \chi_2 \frac{3}{\lambda^4}\phi^{(1)}\frac{\partial \phi^{(1)}}{\partial \xi} - \frac{1}{\lambda^2}\frac{\partial \phi^{(2)}}{\partial \tau}. \tag{3.22}$$

Kinetic correction at the second order. Substituting (3.14) into (3.19) gives

$$v\frac{\partial f_j^{(2)}}{\partial \xi} - \frac{Q_j}{\mu_j}\frac{\partial \phi^{(2)}}{\partial \xi}\frac{\partial f_j^{(0)}}{\partial v} = 2C_{ja}^{(2)}\frac{\partial f_j^{(0)}}{\partial v^2} + 4C_{jb}^{(2)} v \frac{\partial^2 f_j^{(0)}}{\partial (v^2)^2}, \tag{3.23}$$

with

$$C_{ja}^{(2)} = \chi_1 \lambda \frac{Q_j}{\mu_j}\frac{\partial \phi^{(1)}}{\partial \xi}, \qquad C_{jb}^{(2)} = \left(\frac{Q_j}{\mu_j}\right)^2 \phi^{(1)}\frac{\partial \phi^{(1)}}{\partial \xi}. \tag{3.24}$$

As before, we retain the regularizing time derivative at $O(\epsilon^{9/2})$ and Fourier transform,

$$\chi_1 \epsilon^2 \frac{\partial f_{j\epsilon}^{(2)}}{\partial \tau} + v\frac{\partial f_j^{(2)}}{\partial \xi} - \frac{Q_j}{\mu_j}\frac{\partial \phi^{(2)}}{\partial \xi}\frac{\partial f_j^{(0)}}{\partial v} = 2C_{ja}^{(2)}\frac{\partial f_j^{(0)}}{\partial v^2} + 4C_{jb}^{(2)} v \frac{\partial^2 f_j^{(0)}}{\partial (v^2)^2}, \tag{3.25}$$

which yields

$$\hat{f}_{j\epsilon}^{(2)} = \frac{Q_j}{\mu_j}\frac{k\,\partial_v f_j^{(0)}}{vk - \chi_1 \epsilon^2 \omega}\hat{\phi}^{(2)} - i\left[\frac{2\hat{C}_{ja}^{(2)}\,\partial_v^2 f_j^{(0)}}{vk - \chi_1 \epsilon^2 \omega} + \frac{4\hat{C}_{jb}^{(2)} v\,\partial_{(v^2)}^2 f_j^{(0)}}{vk - \chi_1 \epsilon^2 \omega}\right], \tag{3.26}$$

and, with $\omega \to \omega + i\gamma$,

$$\hat{f}_{j\epsilon}^{(2)} = \frac{Q_j}{\mu_j}\frac{k\,\partial_v f_j^{(0)}}{(kv - \chi_1 \epsilon^2 \omega) - i\gamma\chi_1\epsilon^2}\hat{\phi}^{(2)} - i\left[\frac{2\hat{C}_{ja}^{(2)}\,\partial_v^2 f_j^{(0)}}{(kv - \chi_1 \epsilon^2 \omega) - i\gamma\chi_1\epsilon^2} + \frac{4\hat{C}_{jb}^{(2)} v\,\partial_{(v^2)}^2 f_j^{(0)}}{(kv - \chi_1 \epsilon^2 \omega) - i\gamma\chi_1\epsilon^2}\right]. \tag{3.27}$$

Transforming back and integrating over velocity (theprincipal value treatment is detailed in Appendix B) gives

$$\frac{\partial n_j^{(2)}}{\partial \xi} = \chi_2 a_j \phi^{(1)}\frac{\partial \phi^{(1)}}{\partial \xi} + \chi_1 b_j \mathcal{P}\int_{-\infty}^{\infty} \frac{\partial \phi^{(1)}(\xi', \tau)}{\partial \xi'}\frac{d\xi'}{\xi - \xi'} - C_j^{(1)}\frac{\partial \phi^{(2)}}{\partial \tau}, \tag{3.28}$$

with $a_j = \theta_j^{-2}$ and

$$b_j = \frac{1}{\sqrt{2\pi}}\frac{\lambda}{\theta_j}\sqrt{\frac{\mu_j}{\theta_j Q_j}}\frac{2\kappa_j}{(2\kappa_j - 3)^{3/2}}\frac{\Gamma(\kappa_j)}{\Gamma(\kappa_j - \frac{1}{2})}.$$

Evolution equation. Eliminating $n_d^{(2)}$ and $n_j^{(2)}$ from (3.21) using (3.22) and (3.28) (together with (3.8) and (3.15)) yields the KdV-type amplitude equation with a Landau (Hilbert transform) damping term:

$$\frac{\partial \psi}{\partial \tau} + A\psi \frac{\partial \psi}{\partial \xi} + B\frac{\partial^3 \psi}{\partial \xi^3} + C\,\mathcal{P}\int_{-\infty}^{\infty} \frac{\partial \psi(\xi',\tau)}{\partial \xi'} \frac{d\xi'}{\xi - \xi'} = 0, \qquad \psi \equiv \phi^{(1)}, \tag{3.29}$$

with coefficients

$$\begin{aligned} A &= \chi_2 \frac{\lambda^3}{2}\left(\frac{3}{\lambda^4} - \sum_j \delta_j a_j\right), \\ B &= \chi_3 \frac{\lambda^3}{2}, \\ C &= \chi_1 \frac{\lambda^3}{2} \sum_j \delta_j b_j. \end{aligned} \tag{3.30}$$

Equation (3.29) is a modified Korteweg–de Vries equation incorporating linear Landau damping. It governs the evolution of the electrostatic potential associated with weakly nonlinear, weakly dispersive dust acoustic solitary waves in a collisionless, unmagnetized plasma composed of negatively charged dust grains and two κ-distributed ion species at different temperatures.

3.1. Landau damping in linear dust acoustic waves

To isolate and detail the Landau damping mechanism for linear dust–acoustic waves (DAWs), we suppress nonlinearity and dispersion in the amplitude equation by setting $A = 0$ and $B = 0$. The evolution law reduces to the Landau-only form

$$\frac{\partial \psi}{\partial \tau} + C\,\mathcal{P}\int_{-\infty}^{\infty} \frac{\partial \psi(\xi',\tau)}{\partial \xi'} \frac{d\xi'}{\xi - \xi'} = 0, \tag{3.31}$$

where the Cauchy principal value encodes the resonant wave–particle interaction. Introducing the Hilbert transform

$$\mathcal{H}\{g\}(\xi) = \frac{1}{\pi}\mathcal{P}\int_{-\infty}^{\infty} \frac{g(\xi')}{\xi - \xi'}\, d\xi', \tag{3.32}$$

Eq (3.31) becomes

$$\frac{\partial \psi}{\partial \tau} + \pi C\,\mathcal{H}\left\{\frac{\partial \psi}{\partial \xi}\right\} = 0. \tag{3.33}$$

Taking the Fourier transform $\hat{\psi}(k,\tau) = \int \psi(\xi,\tau) e^{-ik\xi} d\xi$ and using

$$\mathcal{F}\{\partial_\xi \psi\} = ik\,\hat{\psi}, \qquad \mathcal{F}\{\mathcal{H}[g]\} = -\,i\,\mathrm{sgn}(k)\,\hat{g}, \tag{3.34}$$

Eq (3.33) gives

$$\frac{\partial \hat{\psi}}{\partial \tau} - i\pi C\,\mathrm{sgn}(k)\,(ik)\,\hat{\psi} = 0 \implies \frac{\partial \hat{\psi}}{\partial \tau} + \pi C\,|k|\,\hat{\psi} = 0. \tag{3.35}$$

With $\hat{\psi} \propto e^{-i\omega\tau}$, the dispersion relation follows immediately:

$$\omega = -\,i\,\pi\,k\,C. \tag{3.36}$$

The purely imaginary frequency signals exponential (Landau) damping of the mode amplitude.

Normalized damping rate and parameter dependence. The (normalized) Landau damping rate is therefore

$$|\gamma| \;=\; \pi C \;=\; \chi_1 \pi \frac{\lambda^3}{2} \sum_j \delta_j b_j, \tag{3.37}$$

with λ the linear phase speed, and δ_j, b_j species-dependent weights and velocity-moment factors (given explicitly earlier). The prefactor χ_1 controls the overall damping strength and scales with

$$\chi_1 \;\propto\; \mu_d \;=\; \sqrt{\frac{z_d m_1}{z_1 m_d}}, \tag{3.38}$$

highlighting the role of the ions inertia. A full parametric exploration of $|\gamma|$ is provided in Appendix C, and the numerical section.

In Appendix C we carry out the second-order kinetic calculation in detail. The second-order Vlasov equation contains the sources $\propto \partial_\xi \phi^{(1)}$ and $\propto \phi^{(1)} \partial_\xi \phi^{(1)}$; we retain the regularizing term $\chi_1 \epsilon^2 \partial_\tau f_{j\epsilon}^{(2)}$, use the Fourier transform, and apply the Plemelj/Hilbert procedure. After inverting and integrating over v, we obtain

$$\partial_\xi n_j^{(2)} = \chi_a^j \, \phi^{(1)} \, \partial_\xi \phi^{(1)} + \chi_b^j \, \mathcal{H}\{\partial_\xi \phi^{(1)}\} - C_j^{(1)} \, \partial_\xi \phi^{(2)},$$

which, combined with the fluid/Poisson relations at $O(\epsilon^{5/2})$, yields the modified KdV with the explicit coefficients A, B, C. The emergence of $\mathcal{H}$ follows directly from the principal valuestructure.

3.2. Effect of Landau damping on nonlinear dust acoustic solitons

When $C = 0$, Eq (3.29) reduces to the classical KdV equation and supports the soliton

$$\psi(\xi, \tau) = \Psi \operatorname{sech}^2\!\left(\frac{\xi - U\tau}{W}\right), \qquad \Psi = \frac{3U}{A}, \quad W = \frac{12B}{\Psi A} = \sqrt{\frac{4B}{U}}. \tag{3.39}$$

To incorporate weak Landau damping, we treat C as a small perturbation ($A, B \gg C$) and use adiabatic (collective–coordinate) perturbation theory. By expanding the solution in powers of C and allowing the soliton parameters to evolve slowly,

$$\psi(\eta, \tau; C) = \sum_{i=0}^{\infty} C^i \psi^{(i)} = \psi^{(0)} + C\psi^{(1)} + C^2 \psi^{(2)} + \cdots, \qquad \eta = \frac{\xi - \frac{A}{3}\int_0^\tau \Psi(\tau')\, d\tau'}{W}. \tag{3.40}$$

Substituting into the amplitude equation and collecting equal powers of C yields the perturbed solitary wave

$$\psi(\eta, \tau) = \Psi(\tau) \operatorname{sech}^2\!\left(\frac{\xi - \frac{A}{3}\int_0^\tau \Psi(\tau')\, d\tau'}{W}\right), \tag{3.41}$$

with a slowly varying amplitude

$$\Psi(\tau) = \Psi_0 \left(1 + \frac{\tau}{\tau_0}\right)^{-2}, \qquad \tau_0 \approx \frac{1.37}{C} \sqrt{\frac{3B}{A\Psi_0}}. \tag{3.42}$$

As $C \to 0$, $\Psi(\tau) \to \Psi_0$ and Eq (3.39) is recovered. Thus, Landau damping induces algebraic decay of the soliton's amplitude, a concomitant decrease in its propagation speed, and broadening of the pulse.

4. Parametric analysis

This section investigates how various plasma parameters influence key characteristics of dust acoustic (DA) solitary waves. Specifically, we analyze the behavior of the phase velocity λ, the Landau damping rate $|\gamma|$, the solitary wave's amplitude Ψ, its width W, and the propagation speed U under different nonthermal and compositional conditions of the plasma system.

4.1. Phase velocity behavior

Figure 1 provides a detailed visualization of how the nonlinear dust acoustic (DA) wave's phase velocity λ depends on different plasma conditions, especially the ions velocity distributions and relative species concentrations. Figure 1(a) shows the dependence of λ on the nonthermal indices κ_1 (cold ions) and κ_2 (hot ions). The kappa parameter controls the high-energy tail of the velocity distribution: Smaller κ values correspond to more suprathermal particles, while large κ values represent nearly Maxwellian distributions. At small values of κ_2 (i.e., strongly nonthermal hot ion distributions), λ is significantly reduced. This reduction in phase speed is due to the enhanced population of energetic particles, which weaken the net electrostatic restoring force in the plasma. These suprathermal particles smear out potential differences via rapid motion, thereby dampening the collective oscillations and reducing the speed of wave propagation. As κ_2 increases, indicating a shift toward a thermal Maxwellian distribution, the number of suprathermal particles diminishes. Consequently, the plasma response becomes more ideal, and the phase speed increases, eventually saturating when $\kappa_2 \to \infty$. This saturation corresponds to the classical behavior predicted by fluid models assuming thermal equilibrium. Similarly, increasing κ_1 has a parallel effect: The cold ions become less energetic, which enhances the local charge separation and increases λ. However, the sensitivity of λ to changes in κ_1 is less pronounced than for κ_2, suggesting that the hot ion component exerts a more dominant control over the wave dynamics. Another key feature is the identification of subsonic ($\lambda < 1$) and supersonic ($\lambda > 1$) DA wave regimes. For small values of both κ_1 and κ_2, i.e., in the strongly nonthermal limit, the system supports subsonic waves due to strong damping and energy dispersion. For larger values of κ, where the plasma approaches thermal equilibrium, the phase velocity can surpass unity, resulting in supersonic DA waves. The transition between these regimes is governed primarily by the level of suprathermality in the ion populations.

Figure 1(b) examines how the hot ion to dust density ratio δ_2 and the ion temperature ratio $\theta = T_2/T_1$ influence the phase speed. As δ_2 increases, the contribution of hot ions to the overall pressure in the system becomes more significant. This elevated pressure facilitates stronger restoring forces, leading to a higher λ. The temperature ratio θ enhances this effect: A higher θ implies hotter hot ions, which further increase the effective pressure and, consequently, the phase speed. Notably, even when δ_2 and θ are high, the phase velocity remains subsonic if κ_1 and κ_2 are low. This highlights that the nonthermal nature of the plasma — not just the density and temperature — plays a decisive role in determining the propagation speed of DA waves. Only when the system is close to thermal equilibrium (i.e., large κ values) does the effect of density and temperature become dominant. From Eq (3.16), it is evident that the mass ratio parameters μ_d (dust cold ion inertia) and μ_j (ion cold ion inertia) do not explicitly appear in the phase velocity expression. This suggests that λ is predominantly determined by the electrostatic potential balance, not by the inertial properties of the plasma components. Hence, the ion distributions (through κ_j), temperatures (θ), and density ratios (δ_j) are the critical determinants of wave

speed. Therefore, the phase velocity of nonlinear DA waves is intricately influenced by the thermal and compositional structure of the plasma. Suprathermal effects tend to suppress λ, while higher ion densities and temperatures enhance it — but only under near-Maxwellian conditions. This underscores the importance of accounting for nonthermal distributions in modeling wave dynamics in space and laboratory dusty plasmas.

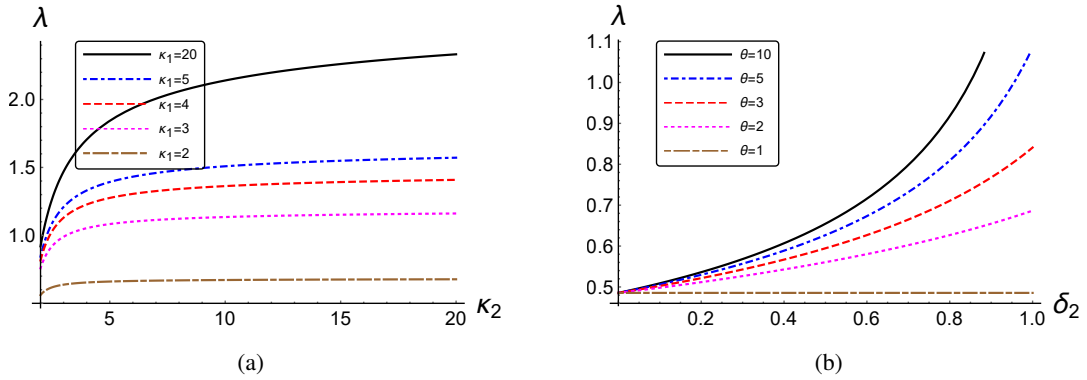

Figure 1. (Color online). Phase velocity λ of the nonlinear DA wave [cf. Eq (3.16)] as a function of: (a) the nonthermal index κ_2 of hot ions for various values of cold ion nonthermality κ_1 (with a fixed $\delta_2 = 0.5$ and $\theta = 2$); (b) the relative hot ion concentration δ_2 for different hot-to-cold ion temperature ratios θ (assuming $\kappa_1 = \kappa_2 = 2$).

4.2. Landau damping rate

Figure 2 explores the sensitivity of the Landau damping rate $|\gamma|$ to key plasma parameters, offering insights into how wave particle resonant interactions are influenced by the system's kinetic structure and mass composition. Figure 2(a) illustrates how $|\gamma|$ varies with the nonthermal indices κ_1 and κ_2, which control the suprathermal tail of the ion velocity distributions. When κ_j is small, the ion population is strongly nonthermal and characterized by a long high-energy tail. In this regime, fewer ions are resonant with the wave, resulting in a relatively small damping rate. Physically, the high-speed ions tend to bypass resonant interaction with the slower-moving wave, reducing energy transfer and damping. As κ_j increases, indicating a shift toward Maxwellian behavior, the number of resonant ions increases, enhancing energy absorption from the wave and thus increasing $|\gamma|$. In the limit $\kappa_j \to \infty$, the system becomes nearly thermal, and the Landau damping rate saturates. This saturation implies a maximal transfer of wave energy to particles under Maxwellian conditions, which is consistent with classical Landau damping theory.

Figure 2(b) examines the effect of increasing the hot to ion density (via δ_2) and the hot cold ion temperature ratio (θ) on $|\gamma|$. Initially, an increase in δ_2 enhances the number of hot ions available for resonant interactions, raising $|\gamma|$. However, beyond a threshold, further increases in hot ion density may disrupt the charge balance and reduce the effective damping. Additionally, higher values of θ imply hotter hot ions, which shift the thermal speed away from the wave speed, reducing probability resonance and thereby diminishing damping. Conversely, lower θ values bring the hot ions thermal speed closer to λ, increasing the overlap in velocity space and enhancing $|\gamma|$.

Figure 2(c) focuses on the role of mass ratios in shaping the damping process. The parameter χ_1

quantifies the ratio of cold ion mass to dust mass and governs the inertia of the cold ions. A larger χ_1 increases the contribution of ionic inertia to the system, enhancing Landau damping as heavier ions more effectively absorb wave energy through resonant processes. The hot to cold ion mass ratio μ has little effect on $|\gamma|$ for small values of χ_1, as the dynamics are dominated by the lighter species and dust. However, as χ_1 grows, the relative importance of μ becomes more pronounced, and $|\gamma|$ increases with an increasing μ. This suggests that the inertial contribution of hot ions to damping becomes significant only when the background (cold ion and dust) system has high inertia itself.

Overall, the Landau damping rate is strongly affected by the kinetic characteristics (nonthermal indices) and mass ratios of the plasma species. While suprathermal effects reduce damping through phase velocity mismatch, increasing thermalization or mass enhances the damping efficiency. This highlights the complex interplay of kinetic distribution, inertia, and resonance conditions in controlling energy dissipation in DA waves.

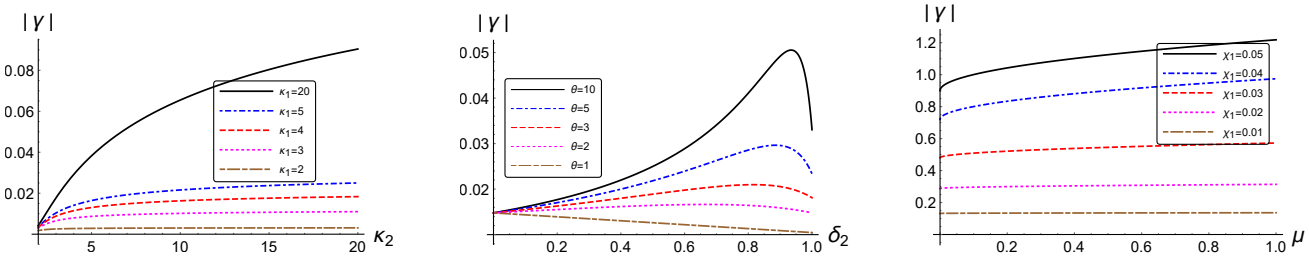

Figure 2. (Color online). Landau damping rate $|\gamma|$ of the nonlinear DA wave [cf. Eq. (3.37)] as a function of: (a) the nonthermal index κ_2 for several values of κ_1 (with $\delta_2 = 0.5$ and $\theta = 2$) , and (b) the hot ion to dust density ratio δ_2 for different ion temperature ratios θ (with $\kappa_1 = \kappa_2 = 2$) , and (c) the hot to cold ion mass ratio μ for various cold ion to dust mass ratios χ_1 (with $\kappa_1 = \kappa_2 = 2$, $\theta = 2$, and $\delta_2 = 0.5$).

Figure 3 illustrates how the solitary wave amplitude $\Psi(\tau)$ evolves over time in response to changes in the nonthermal parameters and mass or density ratios within the plasma.

According to Eq (3.41), the amplitude Ψ determines the width W and propagation speed U of the solitary wave through the relationships $W \propto 1/\sqrt{\Psi}$ and $U \propto \Psi$. Therefore, analyzing how Ψ varies provides insight into how the pulse width and velocity evolve. Figure 3(a) shows the role of the nonthermal indices κ_1 and κ_2. As these indices increase (indicating reduced suprathermality), the amplitude Ψ exhibits a slower decay over time. This means the wave retains its energy for a longer duration in more thermalized plasmas. In contrast, smaller κ values (strongly nonthermal conditions) lead to rapid amplitude attenuation due to enhanced damping via resonant particle wave interactions.

Figure 3(b) displays how the amplitude decay is affected by changes in δ_2 and θ. A reduction in δ_2 (fewer hot ions relative to dust) correlates with less damping and hence a slower amplitude decay. Similarly, increasing the temperature ratio θ accelerates the decay, as hotter hot ions interact more efficiently with the wave due to their higher thermal velocities, thereby extracting more energy from the wave.

Figure 3(c) presents the effect of mass ratios. While changes in μ (hot to cold ion mass ratio) have a limited impact on Ψ when χ_1 is small, the effect becomes significant as χ_1 increases. The parameter

χ_1 (cold ion mass to dust mass ratio) plays a dominant role: Higher values enhance ion inertia, leading to stronger Landau damping and more rapid decay of the solitary wave's amplitude.

In summary, the temporal evolution of the DA solitary wave is highly sensitive to both kinetic and compositional plasma parameters. Nonthermal effects and species inertia control the damping strength, while density and temperature ratios fine-tune the rate of the reduction inamplitude. This highlights the need to account for detailed plasma microphysics in predicting the stability and longevity of electrostatic solitary structures in dusty environments.

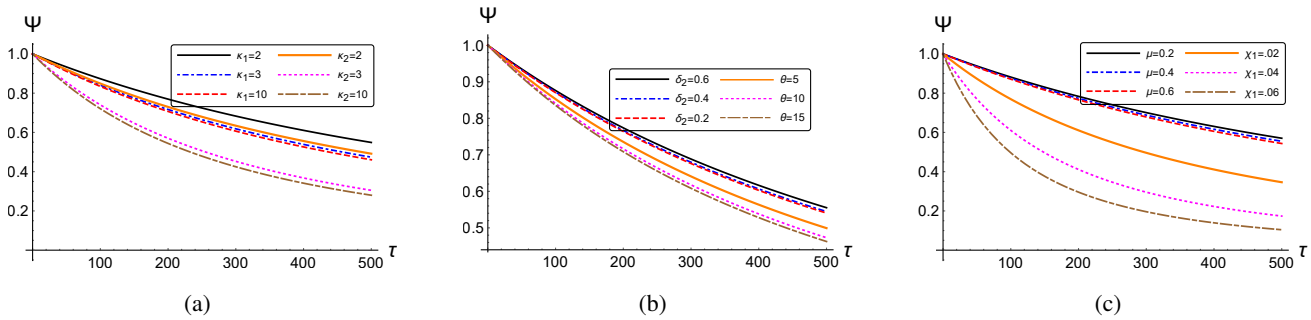

Figure 3. (Color online). Time evolution of the solitary wave's amplitude $\Psi(\tau)$ under various plasma conditions: (a) Effect of nonthermal indices κ_1 and κ_2 ($\delta_2 = 0.5$, $\theta = 2$) , (b) variation of δ_2 and θ ($\kappa_1 = \kappa_2 = 2$) , and (c) influence of the mass ratios μ and χ_1 ($\kappa_1 = \kappa_2 = 2$, $\theta = 2$, $\delta_2 = 0.5$).

5. Astrophysical implications: Enceladus' plume and Saturn's E ring

Saturn's E ring and the active plume of Enceladus constitute a natural laboratory for dusty plasma physics. In this section we connect our Landau–modified KdV framework to Cassini observations by (i) outlining relevant in situ constraints, (ii) mapping observed ranges to the normalized parameters used in our model, and (iii) discussing implications for phase speed, damping, and the persistence of solitons.

5.1. Observational context of Cassini

Cassini's comprehensive payload provides multi-instrument coverage of the E–ring environment and Enceladus' plume. The Cassini Plasma Spectrometer (CAPS) characterizes ion distributions and moments [49], the Radio and plasma wave science (RPWS) instrument probes plasma waves and the ambient electron environment (including Langmuir probe data) [50], and the Cosmic Dust Analyzer (CDA) constrained the dust size distributions and fluxes [51]. Imaging and field/particle datasets established the plume's activity and composition [52–56].

Typical envelopes consistent with these observations are: (a) water–group ion densities ranging from a few to $\sim 10^2\,\mathrm{cm}^{-3}$ in the E–ring region and locally enhanced values within/near plume crossings; (b) characteristic energies/temperatures from sub–eV to a few eV; (c) negatively charged icy grains spanning radii $a \sim 0.05$–$5\,\mu$m with floating potentials of order a few volts, implying charge states $|z_d|$ of ~ 10–10^3 depending on the size and environment; and (d) nonthermal, and suprathermal tails frequently modeled by κ distributions [9, 57]. These envelopes motivate the

electron–depleted approximation locally in dense, dusty regions (electron attachment to grains), for which quasi–neutrality is primarily between ions and negatively charged dust.

5.2. Mapping observations to model parameters

Using the normalization defined in Section 3 and Appendix A, the Cassini–inferred envelopes translate into the dimensionless parameters

- *Composition:* $\delta_j = z_j n_{j0}/(z_d n_{d0})$ is set by the ion mixture and the dust's reference density inferred from CDA fluxes; representative E–ring/plume values yield $\delta_1 + \delta_2 \simeq 1$ under electron depletion.
- *Mass/temperature ratios:* $\mu_j = m_j/m_1$ and $\theta_j = T_j/T_1$ (with T_1hlbeing the colder/heavier ions' temperature) capture CAPS–derived variation; we use $\theta_2/\theta_1 \gtrsim 1$ to represent a hotter, lighter component.
- *Suprathermality:* $\kappa_j \in [2, 6]$ spans moderately strong tails reported in planetary magnetospheres [9, 57].
- *Dust scales:* z_d and n_{d0} determine λ_d and ω_{pd}, hence the dust–acoustic speed $c_s = \omega_{pd}\lambda_d$, anchoring dimensional widths and timescales for comparison with RPWS fluctuation envelopes and plume crossing durations.

5.3. Implications for phase speed, Landau damping, and solitons

Within the present hybrid fluid–kinetic model, the linear phase speed $\lambda = [\delta_1 C_1^{(1)} + \delta_2 C_2^{(1)}]^{-1/2}$ (Eq (4.16)) and the Landau coefficient C (Eq (4.29)) inherit explicit dependences on $(\delta_j, \mu_j, \theta_j, \kappa_j)$ through the integrals defining $C_j^{(1)}$ and b_j. Three robust trends emerge

1) *Suprathermal enhancement of damping.* A lower κ_j (stronger high–energy tails) increases b_j and thus C, yielding a larger linear damping rate $|\gamma| = \pi C$ (Section 4.1). In denser plume filaments, this predicts the shorter persistence of small–amplitude structures and faster decay of narrowband RPWS electrostatic wave packets.
2) *Mass/temperature control of phase speed.* Heavier/colder ion fractions (larger μ_j, smaller θ_j) elevate λ and modify the KdV coefficients (A, B), shifting the balance between steepening and dispersion. This modulates the dimensional soliton width $W \propto \sqrt{B/U}$ and the adiabatic decay timescale $\tau_0 \propto C^{-1}\sqrt{B/(A\Psi_0)}$ (Section 4.3, Appendix D).
3) *Dust charging and composition effects.* Through z_d and n_{d0}, the dust scales are set as c_s and λ_d, thereby fixing the physical length and time scales of solitary structures. Enhanced dust charging (more negative z_d) increases c_s and can promote longer propagation distances before Landau dissipation erodes the amplitude.

Taken together, these trends provide testable links between measured ion/dust properties and (i) the decay envelopes of electrostatic fluctuations, (ii) inferred coherence lengths of compressive structures, and (iii) spatial gradients in fluctuation amplitude across the plume and inner E–ring. We outline specific parameter windows (Sections 4.2 and 4.3) consistent with CAPS/CDA constraints and suggest targeted RPWS diagnostics (e.g., Hilbert–envelope fitting using $|\gamma| = \pi C$) for retrospective analyses.

5.4. Dust charging model

In the Enceladus plume and E–ring environment, the charge carried by a dust grain is set by a balance among competing currents at the grain's surface, including ion collection, (possible) residual electron collection, photoemission, and secondary electron emission. In this work, we adopt a standard orbit-limited–motion (OML) closure, generalized to account for suprathermal (κ-distributed) ion populations, to obtain an effective steady grain potential ϕ_d and charge number $Z_d = 4\pi\epsilon_0 a\phi_d/e$ as functions of the local plasma parameters and grain size. The specific choice is motivated by Cassini-era constraints for densities, temperatures, and grain radii in Saturn's E–ring region and Enceladus' plume; it provides a consistent normalization and parameterization for the hybrid fluid–kinetic model developed below. A full treatment of the charging microphysics (including time-dependent charging, non-spherical grains, material-dependent yields, and detailed κ-dependent collection kernels) is beyond the scope of the present article and will be addressed elsewhere.

5.5. Applicability, limitations, and Landau–damping budget

Our working assumptions (electron depletion, 1D propagation, and weak nonlinearity and dispersion) are most appropriate locally within dense plume filaments and selected E–ring sectors. Magnetic-field effects, grain–charge fluctuations, and strong–amplitude events may require extensions (e.g., magnetized kinetics, time–dependent charging), which we defer to future work. Here, we quantify when ion's Landau damping is relevant for DAWs and when it may be negligible compared to any putative contribution.

In our hybrid closure, the linear Landau damping rate reads

$$|\gamma| \;=\; \pi C \;=\; \frac{\pi\chi_1\,\lambda^3}{2}\;\sum_{j=1}^{2}\delta_j\,b_j(\kappa_j,\mu_j,\theta_j), \tag{5.1}$$

with b_j increasing as suprathermality strengthens (smaller κ_j), and λ is the DAW's phase speed (Section 4). If one were to include a kinetic dust response with thermal speed $v_{\mathrm{th},d} = \sqrt{k_B T_d/m_d}$, the dust's contribution would scale as

$$|\gamma|_d \;\propto\; \left.\frac{\partial f_d}{\partial v}\right|_{v=\lambda} \;\sim\; -\,\frac{\lambda}{v_{\mathrm{th},d}^2}\,\exp\!\left[-\frac{\lambda^2}{2v_{\mathrm{th},d}^2}\right] \quad \text{(Maxwellian estimate)}, \tag{5.2}$$

and an analogous algebraic form for κ-tails (with a power-law rather than exponential decay, still evaluated at $v = \lambda$). For DAWs in electron–depleted mixtures, $\lambda \sim \sqrt{Z_d k_B T_i/m_d}$ is typically much larger than $v_{\mathrm{th},d}$ (cold dust), while it is comparable with the ions' thermal scale $v_{\mathrm{th},i} = \sqrt{k_B T_i/m_i}$. Consequently,

$$\frac{|\gamma|_{\mathrm{ion}}}{|\gamma|_d} \;\sim\; O\!\left[\frac{\sum_j \delta_j\, b_j(\kappa_j,\mu_j,\theta_j)}{b_d(\kappa_d)}\right]\exp\!\left[\frac{\lambda^2}{2v_{\mathrm{th},d}^2}\right] \;\gg\; 1 \quad \text{for} \quad \lambda \gg v_{\mathrm{th},d}, \tag{5.3}$$

i.e., dust resonance is exponentially (or algebraically, for κ_d) suppressed, while ion resonance remains efficient when $\lambda \lesssim$ a few $v_{\mathrm{th},i}$.

Ionic Landau damping remains important provided is

$$\lambda \lesssim \alpha\, v_{\mathrm{th},i}, \quad \kappa_j \text{ moderate (suprathermal tails)}, \quad T_d \ll T_i \Rightarrow v_{\mathrm{th},d} \ll \lambda, \tag{5.4}$$

with $\alpha = O(1\text{–}3)$. In this regime, $b_j(\kappa_j)$ is enhanced, the sum in (5.1) is non-negligible, and the adiabatic soliton decay time $\tau_0 \propto C^{-1}\sqrt{B/(A\Psi_0)}$ decreases. These conditions are consistent with Cassini–inferred envelopes for Enceladus/E–ring plasmas (cold dust, mixed ion temperatures, and evidence for suprathermal ion tails).

Regimes of dominance or negligibility.

- *Ionic damping dominates:* Cold dust ($T_d \to 0$), $\lambda \sim v_{\mathrm{th},i}$, and smaller κ_j (stronger tails). Then $|\gamma| = \pi C$ from (5.1) controls linear decay and the soliton amplitude law $\Psi(\tau) = \Psi_0(1 + \tau/\tau_0)^{-2}$.
- *Ionic damping weakens:* Very large κ_j (near–Maxwellian with weak tails) and $\lambda \gg v_{\mathrm{th},i}$ (strongly superthermal phase speed), which drive $b_j \downarrow$ and suppress resonance.
- *Dust damping is relevant (outside our model's scope):* Only if dust becomes warm enough that $\lambda \sim v_{\mathrm{th},d}$ or if strong stochastic charging broadens the dust's velocity response; neither is expected in the plume/E–ring conditions we target.

In summary, under the electron–depleted, cold–dust conditions emphasized here, ion Landau damping is the appropriate kinetic loss channel for DAWs; dust Landau damping is parametrically suppressed. Within these constraints, the Landau–modified KdV model offers a transparent, parameter–controlled bridge from microphysics (suprathermal ions, dust charging) to observables (phase speed, damping rate, soliton persistence) in the Enceladus/E–ring system.

6. Summary and conclusions

In this work, we have presented a detailed investigation into the role of Landau damping on the behavior of DAWs in an unmagnetized, collisionless plasma system composed of negatively charged dust grains and two ion populations with differing thermal properties. The ions are assumed to obey a generalized power–law κ distribution function, which accounts for the presence of suprathermal particles commonly found in space and astrophysical plasmas. By employing a hybrid fluid–kinetic model—where the dusty species are treated using fluid dynamics and the ions are described via the Vlasov–Poisson framework—we have examined the propagation characteristics of weakly nonlinear and weakly dispersive DAWs. Through the reductive perturbation method, we derived a modified Korteweg–de Vries (mKdV)–like equation incorporating a nonlocal Hilbert transform term that accounts for the linear Landau damping of cold ions.

Our analysis reveals that the phase velocity of DAWs decreases with increasing suprathermality (i.e., smaller κ), due to enhanced kinetic dispersion caused by the high–energy tails of the ion distributions. In contrast, increasing the ion density ratio δ_2 tends to accelerate the wave, suggesting a strong dependence of collective wave behavior on charge–separation effects and the effective plasma inertia. We derived an analytical expression for the Landau damping rate $|\gamma|$, which is shown to be sensitive to multiple plasma parameters. It increases with the nonthermal κ_j (approaching a saturated Maxwellian limit), the density ratio δ_2, the ion temperature ratio θ, and the hot–to–cold ion mass ratio μ. These dependencies reflect the enhanced phase–space overlap between wave and particles under more thermalized and massive–species conditions, increasing the efficiency of energy exchange. To

explore the nonlinear regime, we implemented an approximate perturbative method to solve the mKdV equation in the presence of weak damping. This yielded solitary–wave solutions whose amplitudes decay with time due to Landau damping. The relations among the waves' amplitude Ψ, width W, and speed U—specifically, $W \propto 1/\sqrt{\Psi}$ and $U \propto \Psi$—were established.

Further, we analyzed how various plasma parameters influence the solitary–wave's profile. We found that the amplitude decays more rapidly with increasing κ_j, θ, and μ, consistent with stronger damping under more inertial and thermalized conditions. On the other hand, increasing the density ratio δ_2 enhances wave's amplitude, likely due to improved charge separation and reduced effective damping. Overall, this study highlights the intricate interplay of kinetic effects, species composition, and nonlinear dynamics in governing the evolution of electrostatic solitary structures in dusty plasmas. Our results are applicable to a range of laboratory, space, and astrophysical environments, such as planetary rings, cometary tails, and plasma sheaths, where nonthermal features and damping processes are prevalent. These findings provide a theoretical basis for diagnosing plasma conditions through wave observations and pave the way for future experimental and numerical investigations.

Motivated by Cassini measurements indicating electron–depleted, dust–rich regions with mixed hot–cold ion populations and suprathermal tails, we added a dedicated section on the astrophysical implications. There we compile representative envelopes for densities, temperatures, grain sizes/charges, and flow speeds and map them onto our normalized parameters $(\delta_j, \theta_j, \mu_j, \kappa_j)$ and the coefficients (A, B, C). The resulting phase speeds λ and damping rates $|\gamma| = \pi C$ lie in regimes that are consistent with observed low–frequency electrostatic fluctuations and intermittent density structures. In particular, (i) enhanced suprathermality (smaller κ_j) inferred in plume–crossing intervals shortens the soliton's persistence time $\tau_0 \sim (C^{-1})\sqrt{B/(A\Psi_0)}$, favoring rapidly decaying pulses; (ii) higher heavy–ion fractions (larger δ_2) and moderate temperature ratios increase λ while leaving a measurable damping imprint through C; and (iii) dust charging levels compatible with OML estimates yield $c_s = \omega_{pd}\lambda_d$ values that set the absolute scales for speed and width. These links provide testable predictions for wave packets and solitary signatures in the E–ring sector and near–vent plume filaments, and they suggest parameter windows where DAW solitary structures can survive over observable distances before kinetic damping dominates.

Understanding the combined influence of Landau damping and nonthermal distributions is crucial in interpreting the structure and stability of low-frequency plasma modes in both controlled and natural plasma systems. In laboratory settings, accurate modeling of DAWs' behavior can aid in plasma confinement, diagnostics, and designing experiments that simulate space–plasma conditions. In space physics, these insights help explain the formation and decay of electrostatic solitary structures, energy transport, and wave–particle interactions in planetary magnetospheres, interplanetary shocks, and dusty plasma environments like cometary tails or Saturn's rings. As space missions increasingly gather in–situ plasma data with a high temporal resolution, the presence of nonthermal distributions and anomalous damping can significantly affect wave–based plasma diagnostics. Our model offers a foundational framework to assess these effects and interpret data from missions such as Cassini, Parker Solar Probe, and future lunar or Martian plasma diagnostics. Hence, this study contributes not only to fundamental plasma theory but also to practical diagnostics and control of plasmas in varied contexts. Future extensions—magnetized kinetics, time–dependent charging, multidimensionality, and direct comparisons with dedicated numerical Vlasov–fluid simulations—are straightforward within the present normalization and will sharpen quantitative connections to observations.

Use of AI tools declaration

The authors declare they have not used artificial intelligence (AI) tools in the creation of this article.

Funding

This research work was funded by Umm Al-Qura University, Saudi Arabia, under grant number 25UQU4340344GSSR03.

Acknowledgments

The authors extend their appreciation to Umm Al-Qura University, Saudi Arabia, for funding this research work through grant number 25UQU4340344GSSR03.

Conflict of interest

The authors declare there is no conflict of interest.

References

1. G. Livadiotis, Introduction to special section on origins and properties of kappa distributions: Statistical background and properties of kappa distributions in space plasmas, *J. Geophys. Res.: Space Phys.*, **120** (2015), 1607–1619. https://doi.org/10.1002/2014JA020825
2. S. Perri, F. Pucci, F. Malara, G. Zimbardo, On the power-law distribution of pitch-angle scattering times in solar wind turbulence, *Sol. Phys.*, **294** (2019), 34. https://doi.org/10.1007/s11207-019-1421-y
3. S. M. Shaaban, M. Lazar, R. Schlickeiser, Electromagnetic ion cyclotron instability stimulated by the suprathermal ions in space plasmas: A quasi-linear approach, *Phys. Plasma*, **28** (2021), 022103. https://doi.org/10.1063/5.0035798
4. M. Lemoine, M. A. Malkov, Power-law spectra from stochastic acceleration, *Mon. Not. R. Astron. Soc.*, **499** (2020), 4972–4983. https://doi.org/10.1093/mnras/staa3131
5. N. Kumar, B. Reville, Nonthermal particle acceleration at highly oblique nonrelativistic shocks, *Astrophys. J. Lett.*, **921** (2021), L14. https://doi.org/10.3847/2041-8213/ac30e0
6. M. Lazar, H. Fichtner, *Kappa Distributions–From Observational Evidences via Controversial Predictions to a Consistent Theory of Nonequilibrium Plasmas*, Cham: Springer International Publishing, (2021), 107–123. https://doi.org/10.1007/978-3-030-82623-9
7. G. Livadiotis, *Kappa Distributions: Theory and Applications in Plasmas*, Elsevier, 2017.
8. V. Vasyliunas, J. Geophys, A survey of low-energy electrons in the evening sector of the magnetosphere with OGO 1 and OGO 3, *J. Geophys. Res.*, **73** (1968), 2839–2884. https://doi.org/10.1029/JA073i009p02839

9. V. Pierrard, M. Lazar, Kappa distributions: theory and applications in space plasmas, *Sol. Phys.*, **267** (2010), 153–174. https://doi.org/10.1007/s11207-010-9640-2
10. I. Kourakis, S. Sultana, M. A. Hellberg, Dynamical characteristics of solitary waves, shocks and envelope modes in kappa-distributed non-thermal plasmas: an overview, *Plasma Phys. Controlled Fusion*, **54** (2012), 124001. https://doi.org/10.1088/0741-3335/54/12/124001
11. I. S. Elkamash, I. Kourakis, Multispecies plasma expansion into vacuum: The role of secondary ions and suprathermal electrons, *Phys. Rev. E*, **94** (2016), 053202. https://doi.org/10.1103/PhysRevE.94.053202
12. M. Lazar, V. Pierrard, S. M. Shaaban, H. Fichtner, S. Poedts, Dual Maxwellian-Kappa modeling of the solar wind electrons: new clues on the temperature of Kappa populations, *Astron. Astrophys.*, **602** (2017), A44. https://doi.org/10.1051/0004-6361/201630194
13. G. Slathia, R. Kaur, N. S. Saini, Interaction of ion acoustic multi-solitons in a magnetised superthermal plasma in the presence of dust, *Chin. J. Phys.*, **89** (2024), 302–314. https://doi.org/10.1016/j.cjph.2024.03.029
14. P. S. Abishek, M. Michael, Ion-acoustic shock waves in a multi-ion plasma of Saturn's magnetosphere with superthermal electrons and ions, *Phys. Plasma*, **32** (2025), 042301. https://doi.org/10.1063/5.0255531
15. R. Jahangir, S. Ali, B. Eliasson, Beam-driven electron-acoustic waves in auroral region of magnetosphere with superthermal trapped electrons, *Phys. Fluids*, **37** (2025), 027108. https://doi.org/10.1063/5.0249424
16. P. K. Shukla, A. A. Mamun, *Introduction to Dusty Plasma Physics*, CRC press, 2015. https://doi.org/10.1201/9781420034103
17. F. Verheest, *Waves in Dusty Space Plasmas*, Springer Dordrecht, 2000. https://doi.org/10.1007/978-94-010-9945-5
18. R. Merlino, Dusty plasmas: from Saturn's rings to semiconductor processing devices, *Adv. Phys.: X*, **6** (2021), 1873859. https://doi.org/10.1080/23746149.2021.1873859
19. A. A. Mamun, The new physics of dust in plasmas, *J. Phys. Conf. Ser.*, **1718** (2021), 012004. https://doi.org/10.1088/1742-6596/1718/1/012004
20. C. Y. Chang, *ULSI Technology*, McGraw-Hill, 1996.
21. D. M. Manos, D. L. Flamm, *Plasma Etching: An Introduction*, Academic Press, 1989.
22. M. A. Lieberman, A. J. Lichtenberg, *Principles of Plasma Discharges and Materials Processing*, John Wiley & Sons, 2005. https://doi.org/10.1002/0471724254
23. N. N. Rao, P. K. Shukla, M. Y. Yu, Dust-acoustic waves in dusty plasmas, *Planet. Space Sci.*, **38** (1990), 543–546. https://doi.org/10.1016/0032-0633(90)90147-I
24. P. K. Shukla, V. P. Silin, Dust ion-acoustic wave, *Phys. Scr.*, **45** (1992), 508. https://doi.org/10.1088/0031-8949/45/5/015
25. M. Rosenberg, R. L. Merlino, Ion-acoustic instability in a dusty negative ion plasma, *Planet. Space Sci.*, **55** (2007), 1464–1469. https://doi.org/10.1016/j.pss.2007.04.012

26. A. P. Misra, N. C. Adhikary, P. K. Shukla, Ion-acoustic solitary waves and shocks in a collisional dusty negative-ion plasma, *Phys. Rev. E*, **86** (2012), 056406. https://doi.org/10.1103/PhysRevE.86.056406

27. I. S. Elkamash, I. Kourakis, Electrostatic shock structures in dissipative multi-ion dusty plasmas, *Phys. Plasma*, **25** (2018), 062104. https://doi.org/10.1063/1.5029322

28. I. S. Elkamash, Electrostatic solitary structures in warm multi-ion dusty plasmas: The effect of an external magnetic field and nonthermal electrons, *Phys. Plasma*, **27** (2020), 022112. https://doi.org/10.1063/1.5139195

29. S. K. Mishra, On the possibility of dust acoustic waves over sunlit lunar surface, *Mon. Not. R. Astron. Soc.*, **503** (2021), 3965–3974. https://doi.org/10.1093/mnras/stab495

30. B. T. Tsurutani, G. S. Lakhina, Some basic concepts of wave-particle interactions in collisionless plasmas, *Rev. Geophys.*, **35** (1997), 491–501. https://doi.org/10.1029/97RG02200

31. A. Antoniazzi, G. D. Ninno, D. Fanelli, A. Guarino, S. Ruko, Wave-particle interaction: from plasma physics to the free-electron laser, *J. Phys. Conf. Ser.*, **7** (2005), 143. https://doi.org/10.1088/1742-6596/7/1/012

32. R. Koch, Wave–particle interactions in plasmas, *Plasma Phys. Controlled Fusion*, **48** (2006), B329. https://doi.org/10.1088/0741-3335/48/12B/S31

33. A. P. Misra, G. Brodin, Wave-particle interactions in quantum plasmas, *Rev. Mod. Plasma Phys.*, **6** (2022), 5. https://doi.org/10.1007/s41614-022-00063-7

34. L. D. Landau, On the vibrations of the electronic plasma, in *Collected Papers of L.D. Landau*, (1965), 445–460. https://doi.org/10.1016/B978-0-08-010586-4.50066-3

35. E. Ott, R. Sudan, Nonlinear theory of ion acoustic waves with Landau damping, *Phys. Fluids*, **12** (1969), 2388–2394. https://doi.org/10.1063/1.1692358

36. A. Bandyopadhyay, K. P. Das, Effect of Landau damping on ion-acoustic solitary waves in a magnetized nonthermal plasma with warm ions, *Phys. Plasma*, **9** (2002), 465–473. https://doi.org/10.1063/1.1427022

37. A. Bandyopadhyay, K. P. Das, Effect of Landau damping on kinetic Alfven and ion-acoustic solitary waves in a magnetized nonthermal plasma with warm ions, *Phys. Plasmas*, **9** (2002), 3333–3340. https://doi.org/10.1063/1.1490132

38. Y. Saitou, Y. Nakamura, Ion-acoustic soliton-like waves undergoing Landau damping, *Phys. Lett. A*, **343** (2005), 397–402. https://doi.org/10.1016/j.physleta.2005.06.035

39. S. Ghosh, R. Bharuthram, Ion acoustic solitary wave in electron-positron-ion plasma: effect of Landau damping, *Astrophys. Space Sci.*, **331** (2011), 163–168. https://doi.org/10.1007/s10509-010-0443-6

40. A. Barman, A. P. Misra, Landau damping effects on dust-acoustic solitary waves in a dusty negative-ion plasma, *Phys. Plasma*, **21** (2014), 073708. https://doi.org/10.1063/1.4890571

41. A. Barman, A. P. Misra, Effects of Landau damping on ion-acoustic solitary waves in a semiclassical plasma, *Phys. Plasma*, **24** (2017), 052116. https://doi.org/10.1063/1.4983308

42. A. Sikdar, M. Khan, Effects of Landau damping on finite amplitude low-frequency nonlinear waves in a dusty plasma, *J. Theor. Appl. Phys.*, **11** (2017), 137–142. https://doi.org/10.1007/s40094-017-0248-x

43. Y. Ghai, N. S. Saini, B. Eliasson, Landau damping of dust acoustic solitary waves in nonthermal plasmas, *Phys. Plasma*, **25** (2018), 013704. https://doi.org/10.1063/1.5011005

44. S. Dalui, A. Bandyopadhyay, Effect of Landau damping on ion acoustic solitary waves in a collisionless unmagnetized plasma consisting of nonthermal and isothermal electrons, *Indian J. Phys.*, **95** (2021), 367–381. https://doi.org/10.1007/s12648-020-01731-5

45. A. Misra, D. Chatterjee, G. Brodin, Landau damping of electron-acoustic waves due to multi-plasmon resonances, *Phys. Plasma*, **28** (2021), 112102. https://doi.org/10.1063/5.0061716

46. H. Mushtaq, K. Singh, S. Zaheer, I. Kourakis, Nonlinear ion-acoustic waves with Landau damping in non-Maxwellian space plasmas, *Sci. Rep.*, **14** (2024), 13005. https://doi.org/10.1038/s41598-024-63773-7

47. J. E. Wahlund, M. Andre, A. I. E. Eriksson, M. Lundberg, M. W. Morooka, M. Shafq, et al., Detection of dusty plasma near the E-ring of Saturn, *Planet. Space Sci.*, **57** (2009), 1795–1806. https://doi.org/10.1016/j.pss.2009.03.011

48. M. W. Morooka, J. E. Wahlund, A. I. Eriksson, W. M. Farrell, D. A. Gurnett, W. S. Kurth, et al., Dusty plasma in the vicinity of Enceladus, *J. Geophys. Res.: Space Phys.*, **116** (2011). https://doi.org/10.1029/2011JA017038

49. D. T. Young, J. Berthelier, M. Blanc, J. L. Burch, A. J. Coates, R. Goldstein, et al., Cassini plasma spectrometer investigation, *Space Sci. Rev.*, **114** (2004), 1–112. https://doi.org/10.1007/s11214-004-1406-4

50. D. A. Gurnett, W. S. Kurth, D. L. Kirchner, G. B. Hospodarsky, T. F. Averkamp, P. Zarka, et al., The Cassini radio and plasma wave investigation, *Space Sci. Rev.*, **114** (2004), 395–463. https://doi.org/10.1007/s11214-004-1434-0

51. R. Srama, T. J. Ahrens, N. Altobelli, S. Auer, J. G. Bradley, M. Burton, et al., The Cassini cosmic dust analyzer, *Space Sci. Rev.*, **114** (2004), 465–518. https://doi.org/10.1007/s11214-004-1435-z

52. C. C. Porco, P. Helfenstein, P. C. Thomas, A. P. Ingersoll, J. Wisdom, R. West, et al., Cassini observes the active south pole of Enceladus, *Science*, **311** (2006), 1393–1401. https://doi.org/10.1126/science.1123013

53. M. K. Dougherty, K. K. Khurana, F. M. Neubauer, C. T. Russell, J. Saur, J. S. Leisner, et al., Identification of a dynamic atmosphere at Enceladus with the Cassini magnetometer, *Science*, **311** (2006), 1406–1409. https://doi.org/10.1126/science.1120985

54. J. H. Waite, M. R. Combi, W. H. Ip, T. E. Cravens, R. L. McNutt, W. Kasprzak, et al., Cassini ion and neutral mass spectrometer: Enceladus plume composition and structure, *Science*, **311** (2006), 1419–1422. https://doi.org/10.1126/science.1121290

55. R. L. Tokar, R. E. Johnson, M. F. Thomsen, D. H. Pontius, W. S. Kurth, F. J. Crary, et al., The interaction of the atmosphere of Enceladus with Saturn's plasma, *Science*, **311** (2006), 1409–1412. https://doi.org/10.1126/science.1121061

56. F Spahn, J. Schmidt, N. Albers, M. Hörning, M. Makuch, M. Seiss, et al., Cassini dust measurements at Enceladus and implications for the origin of the E ring, *Science*, **311** (2006), 1416–1418. https://doi.org/10.1126/science.1121375

57. G. Livadiotis, D. J. McComas, Understanding kappa distributions: A toolbox for space science and astrophysics,*Space Sci. Rev.*, **175** (2013), 183–214. https://doi.org/10.1007/s11214-013-9982-9

Appendix

A. Step-by-step normalization

A.1 Dimensional model and symbols

We start from the one-dimensional, collisionless, unmagnetized dusty plasma model (no electrons), composed of a cold, negatively charged dust fluid and two ion species:

$$\frac{\partial \tilde{n}_d}{\partial \tilde{t}} + \frac{\partial}{\partial \tilde{x}}(\tilde{n}_d \tilde{u}_d) = 0, \tag{A.1}$$

$$m_d \tilde{n}_d \left(\frac{\partial \tilde{u}_d}{\partial \tilde{t}} + \tilde{u}_d \frac{\partial \tilde{u}_d}{\partial \tilde{x}} \right) = - q_d \tilde{n}_d \frac{\partial \tilde{\phi}}{\partial \tilde{x}}, \qquad q_d = -z_d e, \tag{A.2}$$

$$\frac{\partial^2 \tilde{\phi}}{\partial \tilde{x}^2} = -\frac{1}{\epsilon_0} \left(q_1 \tilde{n}_1 + q_2 \tilde{n}_2 + q_d \tilde{n}_d \right), \qquad q_j = z_j e, \ j = 1, 2, \tag{A.3}$$

For each ion species $j \in \{1, 2\}$, the Vlasov equation is

$$\frac{\partial \tilde{f}_j}{\partial \tilde{t}} + \tilde{v} \frac{\partial \tilde{f}_j}{\partial \tilde{x}} - \frac{q_j}{m_j} \frac{\partial \tilde{\phi}}{\partial \tilde{x}} \frac{\partial \tilde{f}_j}{\partial \tilde{v}} = 0, \qquad \tilde{n}_j(\tilde{x}, \tilde{t}) = \int_{-\infty}^{\infty} \tilde{f}_j \, d\tilde{v}. \tag{A.4}$$

Quasi-neutrality at equilibrium reads

$$z_1 n_{10} + z_2 n_{20} = z_d n_{d0}. \tag{A.5}$$

A.2 Scales and normalization map

We introduce the standard dust scales

$$\lambda_d = \sqrt{\frac{\epsilon_0 K_B T_1}{z_d e^2 n_{d0}}}, \quad \omega_{pd} = \sqrt{\frac{z_d^2 e^2 n_{d0}}{\epsilon_0 m_d}}, \quad c_s = \omega_{pd} \lambda_d = \sqrt{\frac{z_d K_B T_1}{m_d}}, \tag{A.6}$$

and the ion thermal speeds

$$v_{\mathrm{th}j} = \sqrt{\frac{K_B T_j}{m_j}}, \qquad j = 1, 2. \tag{A.7}$$

The *normalization map* (dimensional → dimensionless) is

$$\tilde{x} = \lambda_d \, x, \quad \tilde{t} = \frac{t}{\omega_{pd}}, \quad \tilde{u}_d = c_s \, u_d, \quad \tilde{\phi} = \frac{K_B T_1}{e} \, \phi, \quad \tilde{v} = v_{\mathrm{th}1} \, v, \tag{A.8}$$

$$\tilde{n}_d = n_{d0}\, n_d, \quad \tilde{n}_j = n_{j0}\, n_j, \quad \tilde{f}_j = \frac{n_{j0}}{v_{\mathrm{th}\,j}}\, f_j. \tag{A.9}$$

We also allow for a (large) macroscopic scale L and define

$$\ell = \frac{\lambda_d^2}{L^2}, \qquad Q_j = \frac{z_j}{z_1}, \quad \mu_j = \frac{m_j}{m_1}, \quad \theta_j = \frac{T_j}{T_1}, \qquad \delta_j = \frac{z_j n_{j0}}{z_d n_{d0}}, \tag{A.10}$$

and the dust–ion inertia parameter

$$\mu_d = \sqrt{\frac{z_d m_1}{z_1 m_d}}. \tag{A.11}$$

A.3 Normalized equations

Using (A.8) and (A.9), the dust continuity and momentum equations become

$$\frac{\partial n_d}{\partial t} + \frac{\partial}{\partial x}(n_d u_d) = 0, \tag{A.12}$$

$$\frac{\partial u_d}{\partial t} + u_d \frac{\partial u_d}{\partial x} = \frac{\partial \phi}{\partial x}. \tag{A.13}$$

The Vlasov equation (A.4) transforms to

$$\mu_d \frac{\partial f_j}{\partial t} + v \frac{\partial f_j}{\partial x} - \frac{Q_j}{\mu_j} \frac{\partial \phi}{\partial x} \frac{\partial f_j}{\partial v} = 0, \qquad n_j = \sqrt{\frac{\mu_j}{\theta_j}} \int_{-\infty}^{\infty} f_j \, dv, \tag{A.14}$$

where the density factor $\sqrt{\mu_j/\theta_j}$ arises from $d\tilde{v} = v_{\mathrm{th}1}\, dv$ and $\tilde{f}_j = (n_{j0}/v_{\mathrm{th}\,j}) f_j$. Poisson's equation becomes

$$\ell \frac{\partial^2 \phi}{\partial x^2} = n_d - \sum_{j=1}^{2} \delta_j n_j. \tag{A.15}$$

Equilibrium quasi-neutrality reduces to

$$\delta_1 + \delta_2 = 1. \tag{A.16}$$

A.4 Equilibrium distribution of κ and Maxwellian limit

The normalized equilibrium for ions of species j is

$$f_j^{(0)}(v) = \frac{1}{\sqrt{2\pi}\,(\kappa_j - \frac{3}{2})^{1/2}} \frac{\Gamma(\kappa_j)}{\Gamma(\kappa_j - \frac{1}{2})} \left[1 + \frac{1}{\kappa_j - \frac{3}{2}} \frac{\mu_j}{\theta_j} \frac{v^2}{2}\right]^{-\kappa_j}, \tag{A.17}$$

which tends to Maxwell–Boltzmann equilibrium as $\kappa_j \to \infty$

$$f_j^{(0)}(v) \to \frac{1}{\sqrt{2\pi}} \exp\left(-\frac{\mu_j}{\theta_j} \frac{v^2}{2}\right). \tag{A.18}$$

A.5 Ordering and reductive perturbation scaling

Weak damping, nonlinearity, and dispersion are ordered as

$$\mu_d = \chi_1 \epsilon, \qquad \frac{n_d}{n_{d0}} - 1 = \chi_2 \epsilon, \qquad \ell = \chi_3 \epsilon, \tag{A.19}$$

with $0 < \epsilon \ll 1$ and $O(1)$ coefficients $\chi_{1,2,3}$. The stretched variables are

$$\xi = \epsilon^{1/2}(x - \lambda t), \qquad \tau = \epsilon^{3/2} t. \tag{A.20}$$

The perturbation expansions assign a common amplitude $\chi_2 \epsilon$ to the fluid and potential perturbations (to realize the KdV balance)

$$\begin{aligned} n_d &= 1 + \chi_2 \epsilon\, n_d^{(1)} + \chi_2^2 \epsilon^2\, n_d^{(2)} + \cdots, \\ u_d &= \chi_2 \epsilon\, u_d^{(1)} + \chi_2^2 \epsilon^2\, u_d^{(2)} + \cdots, \\ \phi &= \chi_2 \epsilon\, \phi^{(1)} + \chi_2^2 \epsilon^2\, \phi^{(2)} + \cdots, \\ f_j &= f_j^{(0)} + \chi_2 \epsilon\, f_j^{(1)} + \chi_2^2 \epsilon^2\, f_j^{(2)} + \cdots. \end{aligned} \tag{A.21}$$

Using χ_1 or χ_3 instead of χ_2 in the amplitudes would mix damping/dispersion strengths with the wave's amplitude and spoil the KdV balance.

B. First-order derivation

B.1 $O(\epsilon^{3/2})$ fluid relations

Inserting (A.20) and (A.21) in the continuity and momentum equations and collecting $O(\epsilon^{3/2})$ terms gives

$$-\lambda \frac{\partial n_d^{(1)}}{\partial \xi} + \frac{\partial u_d^{(1)}}{\partial \xi} = 0, \tag{B.1}$$

$$-\lambda \frac{\partial u_d^{(1)}}{\partial \xi} - \frac{\partial \phi^{(1)}}{\partial \xi} = 0. \tag{B.2}$$

Integrating in ξ (bounded perturbations) yields

$$n_d^{(1)} = -\frac{\phi^{(1)}}{\lambda^2}, \qquad u_d^{(1)} = -\frac{\phi^{(1)}}{\lambda}. \tag{B.3}$$

B.2 $O(\epsilon^{3/2})$ kinetic relation and regularization

The first-order Vlasov equation reads

$$v \frac{\partial f_j^{(1)}}{\partial \xi} - \frac{Q_j}{\mu_j} \frac{\partial \phi^{(1)}}{\partial \xi} \frac{\partial f_j^{(0)}}{\partial v} = 0, \tag{B.4}$$

whose direct integration admits an arbitrary ξ-dependent function (resonance ambiguity). Following the standard Landau prescription, we retain a formally higher-order term originating from $\mu_d = \chi_1\epsilon$ and $\partial_t \sim \epsilon^{3/2}\partial_\tau$

$$\chi_1\epsilon^2\frac{\partial f_{j\epsilon}^{(1)}}{\partial\tau} + v\,\frac{\partial f_{j\epsilon}^{(1)}}{\partial\xi} - \frac{Q_j}{\mu_j}\,\frac{\partial\phi^{(1)}}{\partial\xi}\,\frac{\partial f_j^{(0)}}{\partial v} = 0. \tag{B.5}$$

Fourier transform $(\xi,\tau)\mapsto(k,\omega)$ with $\omega\to\omega+i\gamma$, $\gamma>0$, we have

$$\hat{f}_{j\epsilon}^{(1)} = \frac{Q_j}{\mu_j}\,\frac{k\,\partial_v f_j^{(0)}}{(kv-\chi_1\epsilon^2\omega)-i\gamma\chi_1\epsilon^2}\,\hat{\phi}^{(1)}. \tag{B.6}$$

Taking $\epsilon\to 0^+$ and using the Plemelj formula $\lim_{\eta\to0^+}(x\pm i\eta)^{-1} = \mathcal{P}(1/x)\mp i\pi\delta(x)$, we obtain

$$\hat{f}_j^{(1)} = 2\,\frac{Q_j}{\mu_j}\,\frac{\partial^2 f_j^{(0)}}{\partial v^2}\,\hat{\phi}^{(1)}, \qquad\Longrightarrow\qquad f_j^{(1)} = 2\,\frac{Q_j}{\mu_j}\,\frac{\partial^2 f_j^{(0)}}{\partial v^2}\,\phi^{(1)}. \tag{B.7}$$

B.3 First-order densities and phase speed

From the density definition, we have

$$n_j^{(1)} = \sqrt{\frac{\mu_j}{\theta_j}}\int_{-\infty}^{\infty} f_j^{(1)}\,dv = -\,C_j^{(1)}\,\phi^{(1)}, \qquad C_j^{(1)} = \frac{\kappa_j-\frac{1}{2}}{(\kappa_j-\frac{3}{2})^{3/2}}\,\frac{1}{\theta_j}. \tag{B.8}$$

Imposing the $O(\epsilon^{3/2})$ quasi-neutrality $n_d^{(1)} - \sum_j \delta_j n_j^{(1)} = 0$ and using (B.3)–(B.8) yields

$$\lambda = \pm\frac{1}{\sqrt{\sum_{j=1}^{2}\delta_j C_j^{(1)}}} = \pm\frac{1}{\sqrt{\delta_1 C_1^{(1)} + \delta_2 C_2^{(1)}}}. \tag{B.9}$$

This completes the detailed path from Eqs (4.9) to (4.16).

C. Second-order derivation

C.1 Fluid relations at $O(\epsilon^{5/2})$

Collecting $O(\epsilon^{5/2})$ from continuity and momentum gives

$$-\lambda\frac{\partial n_d^{(2)}}{\partial\xi} + \frac{\partial u_d^{(2)}}{\partial\xi} = -\left(\frac{\partial n_d^{(1)}}{\partial\tau} + \frac{\partial}{\partial\xi}[n_d^{(1)}u_d^{(1)}]\right), \tag{C.1}$$

$$-\lambda\frac{\partial u_d^{(2)}}{\partial\xi} - \frac{\partial\phi^{(2)}}{\partial\xi} = -\left(\frac{\partial u_d^{(1)}}{\partial\tau} + u_d^{(1)}\frac{\partial u_d^{(1)}}{\partial\xi}\right), \tag{C.2}$$

which combine (using (B.3)) to

$$\frac{\partial n_d^{(2)}}{\partial\xi} = -\frac{2}{\lambda^3}\frac{\partial\phi^{(1)}}{\partial\tau} + \chi_2\,\frac{3}{\lambda^4}\,\phi^{(1)}\frac{\partial\phi^{(1)}}{\partial\xi} - \frac{1}{\lambda^2}\frac{\partial\phi^{(2)}}{\partial\tau}. \tag{C.3}$$

C.2 Second-order kinetic equation and regularization

The $O(\epsilon^{5/2})$ Vlasov equation takes the form

$$v\,\frac{\partial f_j^{(2)}}{\partial \xi} - \frac{Q_j}{\mu_j}\,\frac{\partial \phi^{(2)}}{\partial \xi}\,\frac{\partial f_j^{(0)}}{\partial v} = \chi_1 \lambda\,\frac{\partial f_j^{(1)}}{\partial \xi} + \frac{Q_j}{\mu_j}\,\frac{\partial \phi^{(1)}}{\partial \xi}\,\frac{\partial f_j^{(1)}}{\partial v}, \tag{C.4}$$

or, after substituting $f_j^{(1)}$ from (B.7),

$$v\,\frac{\partial f_j^{(2)}}{\partial \xi} - \frac{Q_j}{\mu_j}\,\frac{\partial \phi^{(2)}}{\partial \xi}\,\frac{\partial f_j^{(0)}}{\partial v} = 2C_{ja}^{(2)}\,\frac{\partial^2 f_j^{(0)}}{\partial v^2} + 4C_{jb}^{(2)}\,v\,\frac{\partial^2 f_j^{(0)}}{\partial (v^2)^2}, \tag{C.5}$$

with

$$C_{ja}^{(2)} = \chi_1 \lambda\,\frac{Q_j}{\mu_j}\,\frac{\partial \phi^{(1)}}{\partial \xi}, \qquad C_{jb}^{(2)} = \left(\frac{Q_j}{\mu_j}\right)^2 \phi^{(1)} \frac{\partial \phi^{(1)}}{\partial \xi}. \tag{C.6}$$

To regularize the resonance, we retain the time derivative stemming from $\mu_d = \chi_1 \epsilon$ and $\partial_t \sim \epsilon^{3/2}\partial_\tau$, which, in the second-order hierarchy, appears as

$$\chi_1 \epsilon^2 \frac{\partial f_{j\epsilon}^{(2)}}{\partial \tau} + v\,\frac{\partial f_j^{(2)}}{\partial \xi} - \frac{Q_j}{\mu_j}\,\frac{\partial \phi^{(2)}}{\partial \xi}\,\frac{\partial f_j^{(0)}}{\partial v} = 2C_{ja}^{(2)}\,\frac{\partial^2 f_j^{(0)}}{\partial v^2} + 4C_{jb}^{(2)}\,v\,\frac{\partial^2 f_j^{(0)}}{\partial (v^2)^2}. \tag{C.7}$$

Fourier transforming and applying $\omega \to \omega + i\gamma$ yields

$$\begin{aligned}\hat{f}_{j\epsilon}^{(2)} = {} & \frac{Q_j}{\mu_j}\,\frac{k\,\partial_v f_j^{(0)}}{(kv - \chi_1\epsilon^2\omega) - i\gamma\chi_1\epsilon^2}\,\hat{\phi}^{(2)} \\ & - i\left[\frac{2\,\hat{C}_{ja}^{(2)}\,\partial_v^2 f_j^{(0)}}{(kv - \chi_1\epsilon^2\omega) - i\gamma\chi_1\epsilon^2} + \frac{4\,\hat{C}_{jb}^{(2)}\,v\,\partial_{(v^2)}^2 f_j^{(0)}}{(kv - \chi_1\epsilon^2\omega) - i\gamma\chi_1\epsilon^2}\right].\end{aligned} \tag{C.8}$$

C.3 Density response and Hilbert transform

Taking $\epsilon \to 0^+$, inverting the transform, and integrating over v (the principal value for the resonant denominator) gives

$$\frac{\partial n_j^{(2)}}{\partial \xi} = \chi_2\,a_j\,\phi^{(1)}\frac{\partial \phi^{(1)}}{\partial \xi} + \chi_1\,b_j\,\mathcal{P}\int_{-\infty}^{\infty} \frac{\partial \phi^{(1)}(\xi',\tau)}{\partial \xi'}\,\frac{d\xi'}{\xi - \xi'} - C_j^{(1)}\,\frac{\partial \phi^{(2)}}{\partial \tau}, \tag{C.9}$$

with

$$a_j = \frac{1}{\theta_j^2}, \qquad b_j = \frac{1}{\sqrt{2\pi}}\,\frac{\lambda}{\theta_j}\,\sqrt{\frac{\mu_j}{\theta_j Q_j}}\,\frac{2\kappa_j}{(2\kappa_j - 3)^{3/2}}\,\frac{\Gamma(\kappa_j)}{\Gamma(\kappa_j - \frac{1}{2})}. \tag{C.10}$$

C.4 Elimination and the amplitude equation

Combining (C.3) and (C.9) with Poisson's equation at $O(\epsilon^{5/2})$, we have

$$\chi_3\,\frac{\partial^2 \phi^{(1)}}{\partial \xi^2} - n_d^{(2)} + \sum_j \delta_j n_j^{(2)} = 0. \tag{C.11}$$

Eliminating $n_d^{(2)}$, and $n_j^{(2)}$, we obtain the modified KdV with the Landau term

$$\frac{\partial\psi}{\partial\tau} + A\,\psi\,\frac{\partial\psi}{\partial\xi} + B\,\frac{\partial^3\psi}{\partial\xi^3} + C\,\mathcal{P}\int_{-\infty}^{\infty}\frac{\partial\psi(\xi',\tau)}{\partial\xi'}\,\frac{d\xi'}{\xi-\xi'} = 0, \qquad \psi \equiv \phi^{(1)}, \tag{C.12}$$

with coefficients

$$A = \chi_2\,\frac{\lambda^3}{2}\left(\frac{3}{\lambda^4} - \sum_j \delta_j a_j\right), \qquad B = \chi_3\,\frac{\lambda^3}{2}, \qquad C = \chi_1\,\frac{\lambda^3}{2}\sum_j \delta_j b_j. \tag{C.13}$$

C.5 Ordering note for $\epsilon^{9/2}\chi_1\partial_\tau f^{(1)}$

Under $\xi = \epsilon^{1/2}(x-\lambda t)$, $\tau = \epsilon^{3/2}t$, one has $\partial_t \sim \epsilon^{3/2}\partial_\tau$ and $\mu_d = \chi_1\epsilon$, so the kinetic time - derivative scales as $\chi_1\epsilon^{5/2}$ in the first order, i.e., the retained $\chi_1\epsilon^2\partial_\tau f^{(1)}$. In the *second-order* equation, the same contribution appears one order higher once the first-order solution feeds the sources, effectively producing an $\epsilon^{9/2}\chi_1\partial_\tau f^{(1)}$ term in the $O(\epsilon^{5/2})$ balance, as used in (C.7).

D. Adiabatic soliton perturbation

D.1 Unperturbed KdV soliton

For $C = 0$, (C.12) reduces to KdV and admits

$$\psi(\xi,\tau) = \Psi\,\mathrm{sech}^2\!\left(\frac{\xi - U\tau}{W}\right), \qquad \Psi = \frac{3U}{A}, \qquad W = \sqrt{\frac{4B}{U}}. \tag{D.1}$$

D.2 Collective-coordinate ansatz and slow evolution

For weak Landau damping $0 < C \ll A, B$, we use the collective-coordinate method. Let the soliton parameters vary slowly with τ and introduce the co-moving, width-scaled coordinate

$$\eta(\xi,\tau) = \frac{\xi - \Xi(\tau)}{W}, \qquad \Xi(\tau) = \frac{A}{3}\int_0^\tau \Psi(\tau')\,d\tau'. \tag{D.2}$$

Seek a regular expansion in C:

$$\psi(\eta,\tau;C) = \sum_{i=0}^{\infty} C^i\psi^{(i)}(\eta,\tau), \qquad \psi^{(0)}(\eta,\tau) = \Psi(\tau)\,\mathrm{sech}^2\eta. \tag{D.3}$$

Substitution into (C.12), and projection onto the adjoint neutral mode (or equivalently, use of integral invariants of KdV) yields the amplitude evolution law

$$\frac{d}{d\tau}\,\sqrt{\Psi(\tau)} = -\,\frac{C}{\sqrt{12B}}\,\alpha, \qquad \alpha = \frac{\int_{-\infty}^{\infty}\mathrm{sech}^2\eta\,\mathcal{H}\{\partial_\eta\mathrm{sech}^2\eta\}\,d\eta}{\int_{-\infty}^{\infty}\mathrm{sech}^4\eta\,d\eta}, \tag{D.4}$$

where the numerical coefficient α comes from the Hilbert term's projection.* Solving for $\Psi(\tau)$, one obtains

$$\Psi(\tau) = \Psi_0\left(1 + \frac{\tau}{\tau_0}\right)^{-2}, \qquad \tau_0 \approx \frac{1.37}{C}\,\sqrt{\frac{3B}{A\,\Psi_0}}, \tag{D.5}$$

which recovers the unperturbed amplitude Ψ_0 as $C \to 0$.

*Evaluating the integrals gives $\alpha \approx 0.791$, leading to the prefactor 1.37 in τ_0 below.

D.3 Perturbed soliton and kinematics

With $\Psi(\tau)$ given by (D.5), the leading-order soliton is

$$\psi(\xi,\tau) = \Psi(\tau)\,\mathrm{sech}^2\left(\frac{\xi - \frac{A}{3}\int_0^\tau \Psi(\tau')\,d\tau'}{W}\right), \qquad W = \sqrt{\frac{4B}{U}} = \frac{12B}{A\,\Psi(\tau)}. \tag{D.6}$$

Landau damping induces a slow algebraic decay of Ψ, a concomitant reduction in the propagation speed $U \propto \Psi$, and a broadening of the pulse $W \propto \Psi^{-1/2}$.

AIMS Press